JBC Papers in Press. Published on June 14, 2018 as Manuscript RA117.001171
The latest version is at http://www.jbc.org/cgi/doi/10.1074/jbc.RA117.001171

Prion gene paralogs are dispensable for early zebrafish development but have non-additive roles in seizure susceptibility

Patricia L.A. Leighton, Richard Kanyo, Gavin J. Neil, Niall M. Pollock, and W. Ted Allison

From the Department of Biological Sciences and the Centre for Prion & Protein Folding Diseases, University of Alberta, Edmonton Alberta T6G 2E9

Running title: Prion paralogs are dispensable for zebrafish development

To whom correspondence should be addressed: Dr. W. Ted Allison, Department of Biological Sciences, University of Alberta, CW 405 Biological Sciences Center, Edmonton Alberta, Canada, T6G 2E9, telephone: (780) 492-4430, E-mail: ted.allison@ualberta.ca

Keywords: Neurodevelopment, Zebrafish, Prion disease, Transcription activator-like effector nuclease (TALEN), Central nervous system (CNS), PrP^{C}, Gene editing, Excitotoxicity, Neural hyperactivity, Neurodegeneration

ABSTRACT

Normally folded prion protein (PrP^{C}) and its functions in healthy brains remain underappreciated compared to the intense study of its misfolded forms ("prions", PrP^{Sc}) during the pathobiology of prion diseases. This impedes development of therapeutic strategies in Alzheimer and Prion diseases. Disrupting the zebrafish homologs of PrP^{C} has provided novel insights, however mutagenesis of the zebrafish paralog *prp2* did not recapitulate previous dramatic developmental phenotypes, suggesting redundancy with the *prp1* paralog. Here we generated zebrafish *prp1* loss-of-function mutant alleles, and compound *prp1*$^{-/-}$;*prp2*$^{-/-}$ mutants. Zebrafish *prp1*$^{-/-}$ and compound *prp1*$^{-/-}$;*prp2*$^{-/-}$ mutants resemble mammalian *Prnp* knockouts insofar as they lack overt phenotypes, which surprisingly contrasts reports of severe developmental phenotypes when either *prp1* or *prp2* are knocked down acutely. Previous studies suggest that PrP^{C} participates in neural cell development/adhesion, including in zebrafish where loss of *prp2* affects adhesion and deposition pattern of lateral line neuromasts. Contrasting the expectation that functions of *prp1* would be redundant to *prp2*, they appear to have opposing functions in lateral line neurodevelopment. Similarly, loss of *prp1* blunted the seizure susceptibility phenotypes observed in *prp2* mutants, contrasting the expected exacerbation of phenotypes if these prion gene paralogs were serving redundant roles. In sum, prion mutant fish lack the overt phenotypes previously predicted, and instead have subtle phenotypes similar to mammals. No evidence was found for functional redundancy in the zebrafish prion gene paralogs, and the phenotypes observed when each gene is disrupted individually are consistent with ancient functions of prion proteins in neurodevelopment and modulation of neural activity.

Reduced PrP^{C} function(s) are a likely contributor to prion disease progression (despite its loss not being sufficient for disease, reviewed in (1,2)), thus it is important to understand PrP^{C}'s normal physiological functions to devise effective disease therapies. Further, removal of PrP^{C} is considered a promising therapeutic avenue for prion and Alzheimer diseases (3,4), and knowing its function is critical to predicting safety and mitigating detrimental effects of treatment. While the normal functions of PrP^{C} are not well characterized, it is known to interact with numerous extracellular matrix and cell surface proteins including laminin (5) and NCAM (6,7). Further investigation of these interactions revealed participation of PrP^{C} in processes such as neuritogenesis and neurite outgrowth (8-10). Recently, it was also found that PrP^{C} is involved in polysialyation of NCAM during epithelial-to-

mesenchymal transitions (11). Understanding the putative PrP^C functions that are relevant *in vivo* has been hindered by the lack of overt phenotypes in *Prnp* knockout mice (12,13), highlighting the need for alternative *in vivo* systems and methods. Zebrafish have emerged as genetically tractable disease models and can be used to complement studies performed in other model organisms such as rats and mice (reviewed in (14)); here we used zebrafish as a model system to further uncover functions of PrP^C.

Zebrafish possess two copies of the prion gene (15), and this type of duplication relative to mammalian homologs is common due to a whole-genome duplication in the fish lineage. Both paralogs of zebrafish prion genes, *prp1* and *prp2*, are similar in possessing all the recognizable linear domains of mammalian prion proteins (Figure 1 and (15-18); specific gene identifiers are listed in the Methods; see Discussion for dismissal of a putative third paralog). The mammalian and fish homologs do not share high percent identity, as the latter are longer, but both are predicted to have the repeat domains, hydrophobic domains, glycine zippers and post-translational modifications (GPI-anchor, disulphide bridge and N-linked glycosylations) that are present in the canonical mammalian prion protein (15,16,19-21). The functional conservation amongst these genes is strongly supported by experiments where mammalian prion proteins rescue phenotypes observed following disruption of fish prion genes (18,22,23). The reciprocal approach expressing fish PrP^C in mammalian cells demonstrates that fish PrP^C has post-translational modifications (glycosylation) similar to its mammalian homologs (20,24). Predicted protein products of *prp1* and *prp2* are present in zebrafish brain, as detected by proteomics, including at least *prp2* being in synaptosomal preparations (25,26).

We recently engineered mutations of *prp2* and were surprised to observe that the fish developed normally, with phenotypes that included deeply conserved roles in NMDA receptor dysregulation, learning/memory, and seizure susceptibility (16,27). This contrasted several works (including our own) using prion knockdown to produce dramatic early defects and that suggested PrP^C is required for embryonic development (16,22,28). To reconcile this discrepancy, we hypothesized that the two PrP^C paralogs in zebrafish, *prp1* and *prp2*, might have partially redundant roles such that *prp1* was masking phenotypes in our *prp2* mutants. The current work addresses this hypothesis, using targeted mutagenesis to disrupt *prp1*, and seeks to resolve whether PrP^C mutation in zebrafish can fulfill its promise of revealing key roles in neurophysiology and neurodevelopment that have been lacking in similar experiments using *PRNP* knockout mammals.

Indeed previous studies in zebrafish have helped to uncover conserved *in vivo* functions of PrP^C including roles in early development and neuroprotective functions. Transient knockdown of *prp1* with a high dose of *prp1* morpholino (MO) was found to arrest development during gastrulation (18), and at a lower dose caused developmental delay, CNS malformations and apoptosis (22). These phenotypes could be reversed through ectopic delivery of zebrafish and mammalian *Prnp* mRNA (18,22). Similarly, *prp2* morphants had differential expression of genes linked to apoptosis, neurogenesis and embryonic development (29) and exhibited developmental deficits (18,22,29,30). However, ectopic delivery of *prp2* mRNA was not readily able to rescue these developmental phenotypes (18,22,30), thus specificity of *prp2* morpholinos remain unverified. Zebrafish studies have also revealed that PrP^C participates in cell adhesion *in vivo*. *Prp1* knockdown has revealed a role for *prp1* in mediating cell adhesion through E-cadherin and Src kinases (18,23,28). Further, we found that *prp1* and *appa* loss have synergistic roles in neuroprotection and cell adhesion and that PrP^C and APP physically interact (22); thus arguing for a specific niche role for PrP1 in its interaction with APP (Amyloid-β Precursor Protein) that can be extended to mammals and expands the research space for considering a role for PrP^C in Alzheimer disease. Therefore morpholino knockdown of prion paralogs in zebrafish, when accompanied by stringent controls of mRNA rescue, has generated enticing support for novel hypotheses about the role of PrP^C loss-of-function in neurodegenerative diseases (2).

Our first aim was to deploy targeted mutagenesis to engineer *prp1* loss-of-function alleles. We generated two lines of fish with frameshift mutations in *prp1* that are predicted to be null alleles. Both lines of $prp1^{-/-}$ mutants as well

as compound *prp1*$^{-/-}$;*prp2*$^{-/-}$ mutants resembled mouse *Prnp* knockouts in that they appeared overtly normal, except that *prp1*$^{-/-}$ mutants were slightly smaller at larval stages. Interestingly, concerted loss of both *prp1* and *prp2* mutants reversed this reduction in larval size. Similarly, combined loss of *prp1* and *prp2* did not exacerbate defects in neural hyperexcitability and instead led to a blunting of seizure susceptibility phenotypes. We also characterized the lateral line, as this is an accessible site to assess role(s) for PrP^C in cell cohesion during neurodevelopment (30). Rather than *prp1* and *prp2* having the hypothesized redundant roles in neuromast patterning, the lateral line phenotypes in mutants were contrasting and non-additive. Overall this data suggests that *prp1* and *prp2* might have opposing/competing roles in the signalling pathway(s) underlying neurodevelopment and neural excitability in at least some tissues.

RESULTS

prp1 TALENs induced somatic and germline mutations in prp1—We sought to disrupt function of *prp1* via targeted mutagenesis, by targetting the 5' end of the first (and only) coding exon with Tal Effector Nucleases (TALENs; custom restriction enzymes designed to engineer double stranded DNA breaks), such that small insertions or deletions producing frame-shift mutations would lead to loss of all predicted protein domains (Figure 1). To ensure that TALENs were capable of producing mutations *in vivo*, we first analyzed somatic cutting in embryos injected with the *prp1* TALEN reagents. High resolution melt analysis (HRM) on genomic DNA from 3 pools of 20 injected embryos revealed different melt profiles compared to the uninjected controls. Somatic cutting of the target genomic DNA was confirmed, in that cloning and HRM analysis on 12 of these clones identified 2 clones (17%) where sequencing revealed 1 or 6 base pair deletions (Supplementary Figure S1A).

Germline transmission of similar mutations was observed, allowing us to generate frameshift (predicted null) mutations in the *prp1* gene of adult fish. F0 generation fish showed interesting melt profiles compared to controls (Sample melt profiles shown in Figure S1B). These interesting clones originated from 3 pairs of fish, and sibling fish from these crosses were raised to adulthood and genotyped.

Identification of fish heterozygous for the prp1 ua5003 and ua5004 frameshift alleles—To identify F1 generation fish carrying mutations in *prp1*, 48 of their adult progeny in the F2 generation were fin-clipped; these were progeny of fish injected with *prp1* TALENS as above. Two males and 3 females had different HRM melt profiles than the controls. Upon sequencing clones from these individual fish, it was found that one male had an 8 bp deletion and an I10T missense mutation (designated as allele **ua5003**, Figure 1A) whereas 3 females and 1 male had a 19 bp deletion (designated as allele **ua5004**, Figure 1A). "ua" in our allele names is the identifier assigned by ZFin.org, the Zebrafish Model Organism Database, to denote "University of Alberta". These frameshift alleles are predicted to produce truncated, nonsense proteins (Figure 1C) that lack all recognizable domains of the mature prion protein.

Both prp1 mutant alleles appear to be phenotypically normal, except being slightly smaller than prp1$^{+/+}$ *at larval stages*—To test whether *prp1* is required for zebrafish development, we bred fish with the *prp1*$^{ua5003/ua5003}$ or *prp1*$^{ua5004/ua5004}$ alleles to homozygosity. We observed no overt phenotypes at larval stages (Figure 1B). Post-larval growth and maintenance also appeared normal, such that adult zygotic mutants were indistinguishable from wild type (adult fish with the ua5003 or ua5004 alleles are shown in Supplementary Figure S2B-C). To test the hypothesis that maternally provided *prp1* mRNA is sufficient to mask early developmental phenotypes, we raised homozygous maternal zygotic mutants for the *prp1* ua5003 and ua5004 alleles. Again, we observed no overt phenotypes (Figure 2), except that *prp1*$^{-/-}$ maternal zygotic mutants with the ua5003 and ua5004 alleles were, respectively, approximately 3% and 2.5% shorter than *prp1*$^{+/+}$ fish at 50 hours post fertilization (hpf) (Figure 2B; $p<0.05$). Thus reduced body size is a consistent phenotype across two independent disruptions of *prp1*, but its biological significance (if any) remains to be determined.

Maternal zygotic prp1$^{-/-}$ *fish have reduced prp1 transcript abundance*—Since we did not observe overt phenotypes in our *prp1* mutants as has been observed in *prp1* morphants (18,22), we

tested the alternate hypothesis that the *prp1* alleles were not null alleles. We found that *prp1* transcript abundance was reduced 10-fold in 3 dpf maternal zygotic *prp1*$^{ua5003/ua5003}$ larvae compared to wild type (Figure 2E, p=0.0027). On the other hand, *prp2* transcript abundance was not altered in these *prp1*$^{ua5003/ua5003}$ larvae (Figure 2F; though note that *prp2* transcript abundance is reduced in *prp2* mutants, see (16), Figure 2H and Supplemental Figure S2E). Similarly, compound mutant maternal zygotic *prp1*$^{-/-}$;*prp2*$^{-/-}$ larvae had dramatically reduced transcript abundance for both *prp1* and *prp2* compared to wild type (Figure 2G & 2H; n=21; p<0.001). Considering the other allele, *prp1* transcript abundance was reduced in 2 dpf maternal zygotic *prp1*$^{ua5004/ua5004}$ larvae by about 50% compared to wild type larvae (Supplementary Figure S2A, p=0.0012). Overall, it appears that *prp1* transcript levels are reduced in fish with the *prp1 ua5003* and *ua5004* alleles - perhaps through nonsense-mediated decay (31).

These transcripts were characterized further, with special attention to the possibility that the deletions we engineered in mutant *prp1* or *prp2* transcripts might produce unexpected mRNA splicing in ways that might allow functional protein to be produced. Two approaches were used. First, transcripts were characterized with 5'RACE (Rapid amplification of cDNA ends) using gene-specific primers positioned in the middle of the only coding exon of each gene, and positioned 3' of the mutations. Compound *prp1*$^{ua5003/ua5003}$;*prp2*$^{ua5001/ua5001}$ mutant larvae at 2 dpf had *prp1* and *prp2* transcripts with 5' ends that were indistinguishable from wild type in length (Supplemental Figure S10), and this was confirmed via sequencing.

Second, transcripts were characterized by examining the alignment of RNA-Sequencing reads to the chromosomal locations containing *prp1* and *prp2* genes (on chromosomes 10 and 25, respectively); we predicted that any unexpected transcript configuration in the mutants would be revealed by reads aligning outside of the exons, and this would occur differentially in mutant but not in wild type RNA-Seq reads. RNA-Sequencing to a large depth (>41M reads) revealed no out-of-place RNA-Seq reads from *prp1*$^{-/-}$;*prp2*$^{-/-}$ mutants relative to the exons of *prp1* or *prp2* genes (Supplemental Figure S11). Incidentally, the abundance of read alignments (Supplemental Figure S11) independently confirmed that the absolute abundances of both *prp1* and *prp2* transcripts are reduced in *prp1*$^{-/-}$;*prp2*$^{-/-}$ mutants (to 21% and 10% of wild type abundances, respectively, at 3 dpf). Overall, following careful characterization we could find no evidence that *prp1* or *prp2* transcripts in our engineered mutants have any opportunity to make functional protein.

Several attempts to make custom monoclonal and polyclonal antibodies in mice and rabbits, using in-house and commercial services, were not successful in producing reagents that gave specific bands on Western blots; therefore we have been unable to query whether our mutants have reduced abundance of PrP1 protein. The reduced *prp1* transcript abundance, combined with the N-terminal frame-shift deletion that predicts absence of all recognizable prion protein domains (Figure 1C), is strong evidence that mature PrP1 protein is either nearly or completely absent in our maternal zygotic mutants. The same arguments apply for *prp2* likely being a null allele, as we previously reported (16), and data herein (including 5'RACE and RNAseq) strengthen this conclusion.

Maternal zygotic prp1$^{-/-}$;*prp2*$^{-/-}$ *fish have no overt phenotypes*—As neither *prp1*$^{-/-}$ mutants nor *prp2*$^{-/-}$ mutants exhibited overt phenotypes in larval or adult stages, we hypothesized that *prp1* and *prp2* have partially redundant functions in zebrafish development. We therefore created maternal zygotic compound *prp1*$^{-/-}$;*prp2*$^{-/-}$ mutants. These fish did not have overt phenotypes, compared to wild type fish at larval (50 hpf, Figure 3A) or adult (Figure 3C) stages. Considering the second *prp1* allele, maternal zygotic compound *prp1*$^{ua5004/ua5004}$;*prp2*$^{ua5001/ua5001}$ mutants also survive into adulthood without displaying overt phenotypes (Supplemental Figure 2D). Loss of *prp2* also appeared to rescue the smaller size of *prp1*$^{-/-}$ larvae, since compound maternal zygotic *prp1*$^{-/-}$;*prp2*$^{-/-}$ mutants were instead approximately 2% longer than wild type fish at 50 hpf (Figure 3B; p=0.0123).

Loss of prp1 reduces the number of neuromasts in the developing zebrafish posterior lateral line—PrP^{C} has previously been shown to contribute to neurite outgrowth (8,9,32), and transient disruption of the zebrafish *prp2* paralog with either morpholinos or mutagenesis was found

to affect lateral posterior lateral line (PLL) primordium migration and neuromast number (30) using an established alkaline phosphatase staining protocol (33,34). Wild type larvae typically have 5 primary trunk neuromasts and 2-3 terminal neuromasts at the tip of the tail arising from the primI primordium (35) (Figure 4A). In some cases, the 6th primary neuromast is deposited before the primoridum reaches the tip of the tail (36). 2 dpf maternal zygotic *prp1*$^{ua5004/ua5004}$ mutants had fewer trunk neuromasts than age-matched wild type AB strain zebrafish (Supplemental Figure S12A-B, $p<0.05$). To verify this phenotype, we crossed our *prp1 ua5004* allele into the *Tg*(*cldnb:gfp*) line. In this line, GFP labels the cell membranes of all PLL cells including those of the neuromasts, the interneuromast cells, and the migrating primordium (37). The trunk neuromast number was reduced in 50 hpf *cldnb:gfp*-labeled zygotic *prp1*$^{ua5004/ua5004}$ fish and *prp1*$^{+/ua5004}$ fish compared to age-matched *cldnb:gfp*-labeled *prp1*$^{+/+}$ fish (Figure 4C-D, Supplemental Figure S12C, $p<0.05$). The difference in neuromast number between wild type *cldnb:gfp* fish compared to non-transgenic wild type fish stained with alkaline phosphatase is likely attributable in large part to the labeling method. Both mature and immature neuromasts express *gfp* mRNA under the *cldnb* promoter, whereas mature neuromasts produce more alkaline phosphatase, accounting for different absolute counts (33), though note the trends in our phenotypes were consistent regardless of method. To ensure that the observed phenotype was not due to developmental delay, neuromast number was also examined in 3dpf larvae. Again, trunk neuromast number was reduced in *prp1*$^{ua5004/ua5004}$ larvae compared to age-matched wild type AB strain larvae (Figure 4E, $p<0.05$), as assessed through alkaline phosphatase labeling. Upon counter-staining with phalloidin, to more readily visualize the somites and thus document neuromast position, it was found that the L1 neuromast was deposited more posteriorly (near somites 7-8) in 20% of the 3 dpf *prp1*$^{ua5004/ua5004}$ fish compared to the wild type fish examined, wherein the L1 neuromast was deposited near somites 5-6 (although 10% of wild type fish examined on a different day had L1 positioned near somites 7-8 as well; data not shown). Unexpectedly, when we compared the number of neuromasts in 3dpf maternal zygotic *prp1*$^{ua5003/ua5003}$ to age-matched wild type larvae, we found approximately the same number of neuromasts in both genotypes (Figure 4E). For this reason, it is possible that developmental delay contributes to the lateral line phenotype observed in 2dpf *prp1*$^{-/-}$ larvae. Altogether, however, these data support that *prp1* is involved in normal development of the zebrafish PLL.

Loss of prp2 increases the number of neuromasts in the developing zebrafish posterior lateral line—We hypothesized that *prp1* and *prp2* have redundant roles in PLL development, and we expected that loss of *prp2* would also disrupt PLL neuromast deposition. As neuromast patterning was previously found to be disrupted in *prp2* morphants and mutants (30), we examined neuromast position and number in maternal zygotic *prp2*$^{ua5001/ua5001}$ mutants. We previously reported that the L1 neuromast was prematurely deposited in maternal zygotic *prp2*$^{ua5001/ua5001}$ mutants (30). Here we confirmed and extended this conclusion, finding that the L1 neuromast was deposited prematurely (near somites 1-3) in 92% of maternal zygotic *prp2*$^{ua5001/ua5001}$ mutants. In wild type fish, the L1 neuromast was typically found near somites 5-6, with a range between the 3rd-8th somites. Additionally, the maternal zygotic *prp2*$^{ua5001/ua5001}$ mutants had extra primI trunk neuromasts at 3 dpf compared to age-matched wild type AB strain (*prp2*$^{+/+}$) fish (Figure 4E, Supplemental Figure S12D, $p<0.0001$). Comparing this data with that of the previous section, an unexpected contrast emerges: *prp1* promotes neuromast formation and/or deposition, whereas *prp2* restricts the number of neuromasts in the PLL. Our hypothesis that *prp1* and *prp2* principally have redundant roles in PLL development was therefore rejected.

Combined loss of prp1 and prp2 restores the number of posterior lateral line neuromasts to wild type levels—Considering that *prp1* and *prp2* have opposite effects on neuromast abundance when they are lost, as reported above, we next examined whether a genetic interaction between *prp1* and *prp2* might exist in neuromast number and patterning. Heterozygous loss of both *prp1* and *prp2* in 3dpf compound *prp1*$^{+/ua5004}$; *prp2*$^{+/ua5001}$ fish did not disrupt the neuromast number compared to age-matched wild type AB strain (*prp1*$^{+/+}$; *prp2*$^{+/+}$ fish) (Figure 4E).

Additionally, the L1 neuromasts in compound heterozygous *prp1*$^{+/ua5004}$; *prp2*$^{+/ua5001}$ mutants were positioned near somites 4-6, matching the pattern seen in wild type AB strain zebrafish. To further test whether an interaction between *prp1* and *prp2* might exist in neuromast number and patterning, we bred to generate compound homozygous fish. The neuromast number in 3 dpf compound *prp1*$^{ua5003/ua5003}$;*prp2*$^{ua5001/ua5001}$ larvae was also reduced (though not significantly) relative to the number of neuromasts in 3 dpf *prp2*$^{ua5001/ua5001}$ fish (Figure 4E). Overall, concerted loss of *prp1* and *prp2* in *prp1*$^{-/-}$;*prp2*$^{-/-}$ double mutants tended to revert the apparently opposing phenotypes that were observed in single *prp1*$^{-/-}$ and *prp2*$^{-/-}$ mutants; these data further reject our hypothesis that the prion gene paralogs are principally redundant during PLL neurodevelopment.

Combined loss of prp1 and prp2 does not exacerbate seizure susceptibility phenotypes—A role for PrP^{C} in seizures has been debated, due to disparate seizure susceptibility phenotypes in various *Prnp* knockout mice (reviewed in (1,38,39)), which may (or may not) be related to seizures observed in Alzheimer and prion disease patients (40-43). Zebrafish, as a disparate system, contributed to resolving this controversy when it was reported that *prp2*$^{ua5001/ua5001}$ mutant zebrafish larvae have increased susceptibility to convulsant, perhaps via modulating NMDA receptors, amongst other mechanisms (16). We sought to further clarify this issue, and ask if control of neural excitability is a shared function of ancient prion gene products, by investigating if our *prp1* mutants exhibit seizure susceptibility phenotypes. Measuring larval locomotion in response to a low dose range of the convulsant PTZ (pentylenetetrazole) induces stage II seizures resembling a whirling motion as larvae swim erratically around the well of a 96-well plate (Figure 5A) (44). We predicted that loss of *prp1* would increase responses to convulsant, as this appears to be a common effect of PrP^{C} disruption in various systems (though see debate above). We also expected that loss of *prp1* would synergize with loss of *prp2* in this regard, a prediction emanating from our hypothesis that these paralogous genes serve redundant roles.

Larvae lacking *prp1* were found to be more susceptible to the convulsant PTZ compared to wild type (representative example in Figure 5A). This was especially apparent during responses to low doses of PTZ, where maternal zygotic *prp1* mutants had approximately double the activity compared to wild type (Figure 5C; $p<0.05$ at 5mM and 10mM PTZ). Larvae lacking *prp1* did not present with significant changes in basal activity levels (Figure 5D) compared to wild type. This increased susceptibility to convulsant in *prp1* mutants was robust, being apparent when seizure susceptibility was assessed with various methods including swim velocity (Supplemental Figure S7), or when considering a second allele of *prp1* in various metrics of seizure intensity and using altered equipment parameters (Supplemental Figure S8 and see Methods), or when assessing sensitivity to convulsants via measuring abundance of the immediate early gene *c-fos* (Supplemental Figure S9). This seizure susceptibility in *prp1* mutants was reminiscent of phenotypes following loss of *prp2* (see (16) and new data Figure 5 and Supplemental Figures S7 & S9), though lesser in its impact upon the phenotype. Indeed at all doses of convulsant we investigated, loss of *prp2* significantly increased seizure susceptibility above wild type (Figure 5C, $p<0.0001$), and was several-fold more impactful on seizures than loss of *prp1* (Figure 5C).

The similarity of these seizure susceptibility phenotypes is consistent with our hypothesis that *prp1* and *prp2* play redundant roles in regulating neuron excitability. To test this further, we assessed concerted loss of *prp1* and *prp2* and predicted an exacerbation of the seizure phenotype. Contrary to this expectation, compound *prp1*$^{ua5003/ua5003}$;*prp2*$^{ua5001/ua5001}$ larvae were found to have blunted seizure susceptibility compared to the *prp2*$^{ua5001/ua5001}$ larvae at most doses (Figure 5C, Supplemental Figures S7 and S9). Indeed the seizure activity of *prp2*$^{-/-}$ mutants was significantly higher than that of compound *prp1*$^{-/-}$;*prp2*$^{-/-}$ mutants (Figure 5C, $p<0.0001$) at three of the four doses tested. Loss of *prp1* did not significantly impact the baseline stochastic activity levels of larvae, nor did it significantly alter the impact of *prp2* mutation on baseline activity (Figure 5D, Supplemental Figure S7).

In sum, loss of *prp1* increases seizure susceptibility in zebrafish larvae akin to observations on *prp2* mutants made previously (16) and confirmed herein. However the impact of

prp1 and *prp2* on seizures do not appear to be redundant, and instead it appears that loss of *prp1* blunts the impact of *prp2* loss, suggesting opposing actions of these gene products in regulating neural or synaptic activity.

DISCUSSION

Engineering prion mutant zebrafish refines the cadre of conserved functions for prion protein—The functions of PrP^C in healthy brains has remained a matter of interest and debate, in part due to the complexity of its numerous putative functions, and in part due to the potential impact of PrP^C functions being lost during disease or during treatment thereof. Zebrafish, and their purported phenotypes when PrP^C homologs are disrupted, offer very good potential to continue contributing to this debate. Here, we successfully used TALENs to engineer two lines of zebrafish that have frameshift mutations in *prp1,* a homolog of the mammalian gene encoding PrP^C. We also generated compound maternal zygotic *prp1*$^{-/-}$*;prp2*$^{-/-}$ zebrafish, such that all recognizable homologs of PrP^C are predicted to be absent. The lack of overt developmental phenotypes in these zebrafish prion mutants is in line with what has been observed in *Prnp* knockout mice, goats and cattle (12,13,45,46) and in goats with a naturally occurring *Prnp* null allele (47). The phenotypes that were observed in these mutants include defects in neurodevelopment and neurophysiology at the level of seizure susceptibility. The details of these phenotypes suggest conserved, ancient and non-redundant actions of prion genes in these spheres of broad interest for revealing prion protein function and evolution.

Importantly, the mutant phenotypes characterized herein differ substantially in severity from the developmental defects and CNS cell death found by several groups, including our own, in *prp1* morphants (1,2,18,19,21-23,28,48,49). These morphant phenotypes have included defects in cell adhesion and molecular interactions that inform hypotheses about the importance of PrP^C in neurodevelopment and disease. Loss of *prp1*, as induced by high doses of morpholino, is also reported to halt embryo gastrulation, which has been one of several key observations that inspires framework hypotheses about the early evolution of PrP^C homologs from zinc transporter proteins (50-53), and their role in cell adhesion during epithelial-to-mesenchymal transition (11,54-57). The differences between the morphant and mutant phenotypes could be for technical reasons. For example, either: 1] we have not created null alleles; 2] phenotypes in the mutants are masked by maternal wild type transcripts deposited in the egg; or 3] the morpholinos have off-target effects. A separate, biological explanation for the disparity is also important to consider: the acute loss of *Prnp* homologs could produce different phenotypes compared to chronic loss in *Prnp*$^{-/-}$ homolog mutants (e.g. through genetic compensation). In the next paragraphs we consider these alternatives in turn.

First, while we have not definitively demonstrated that we have created null alleles due to lack of suitable antibodies (see Results), the two frameshift mutations we engineered are both predicted to produce truncated proteins lacking all recognizable domains of prion proteins (Figure 1). Further, we report here that the *prp1* transcript levels are substantially reduced in both of our engineered lines of *prp1*$^{-/-}$ mutants (but *prp2* transcript abundance is normal in *prp1* mutants; the reciprocal is also true – only *prp2* is reduced in *prp2* mutants). Because the total abundance of *prp1* in wild type zebrafish larvae is not large (e.g. compared to *prp2*), measuring decreases in abundance begins to be similar to reporting baseline noise when the transcript is absent: a 90% decrease in *prp1* abundance is comparable to decreasing the RT-qPCR signal into the region of the baseline noise. Notably, there is no formal reason to expect the small deletions we engineered (e.g. 8 base pairs deleted, producing a frameshift mutation– see Figure 1) to result in *any* decreased transcript abundance as would be expected following gene knockout. In this context the reduction in *prp1* transcripts, presumably by nonsense-mediated decay, is impressively thorough and perhaps indicates a substantial deficit. Similarly, we previously reported a marked reduction in *prp2* transcript levels in *prp2*$^{ua5001/ua5001}$ fish (16), and that remains apparent in our *prp1*$^{-/-}$;*prp2*$^{-/-}$ fish (independently assessed by RT-qPCR and RNA-Seq). Further, our 5'RACE and RNA-Seq analyses imply that the transcripts made are the predicted loss-of-function alleles, i.e. no unexpected transcript splicing is observed. Thus *prp1*$^{-/-}$;*prp2*$^{-/-}$ fish are expected to have, at minimum, a substantial loss of PrP^C

function via both truncated predicted proteins and decreased abundance: if they are not null mutants then they are reasonably assumed herein to be strong hypomorphs. Arguably, the loss of gene function in the strong hypomorphs ought be comparable to or greater than that produced by morpholino-based gene knockdown. Two independent mutant alleles of *prp1* were generated, each producing a different frameshift in the sole coding exon, and therefore each is predicted to truncate the protein into a different null allele lacking all recognizable prion protein domains (Figure 1). That many of the phenotypes we predicted are indeed observable in our larvae, though not as dramatic as perhaps expected, also argues in favour of gene disruption having been successful. Indeed while the various phenotypes in the *prp1* mutants (neurodevelopment, larval size and seizure susceptibility) seem subtle, they were consistent with predictions and are also robust and specific, insomuch that they can be reversed or blunted in a coordinate manner following disruption of a related gene paralog (*prp2*).

Second, another possible reason for the discrepancy between mutant and morphant phenotypes is that the morpholinos deployed against *prp1* and *prp2* are expected to impact maternally deposited mRNA in the embryo, whereas mutants generated from an incross of heterozygous parents might have wild type transcripts present in their embryos. Indeed maternal zygotic deposition of transcript has been documented for both *prp1* (18) and *prp2* (16). To address this, we generated maternal zygotic embryos by breeding fish that were homozygous mutant for the prion gene paralogs such that the embryos are expected to completely lack wildtype transcript. We completed this for multiple *prp1* alleles by breeding these with fish carrying the *prp2 ua5001* allele. We observed that maternal zygotic embryos were normal in the double $prp1^{ua5003/ua5003}$;$prp2^{ua5001/ua5001}$ mutants, and also with an alternate *prp1* allele generating maternal zygotic $prp1^{ua5004/ua5004}$;$prp2^{ua5001/ua5001}$ embryos. Indeed these maternal zygotic embryos and larvae were viable, and raised to adulthood without displaying overt phenotypes. Therefore it is unlikely that maternal contribution of wild type transcript is masking phenotypes in our mutants, removing this potential difference compared to morphants.

Third, while we and others have presented data that argues strongly in favour of the specificity of the *prp1* morpholinos (MO), some off-target toxicity may yet exist and this would likely be exacerbated upon delivery of higher morpholino doses. Rescue of a morphant phenotype with cognate mRNA is an important control to test for morpholino specificity (58,59). We previously showed that *prp1* morphant phenotypes, using low doses of MO, can be partially rescued by injection of cognate *prp1* mRNA or homologous mammalian *Prnp* mRNA, but not by similar mRNAs encoding *prp2* or *shadoo* (22). Therefore mRNA rescue experiments in past efforts were thorough (thousands of embryos phenotyped in dozens of replicated mRNA + MO rescue combinations; control mRNA injections with engineered STOP codons used, mRNA rescue using paralogs was successful but only in certain contexts, etc.) (22), and are strongly supportive of MO specificity at these low MO doses.

An additional test of MO specificity is to assess the prediction that MO-induced phenotypes will be reduced when the MO is injected into embryos that are loss-of-function mutants for the MO target gene. This strategy was attempted here; we sought to define *prp1* MO specificity by delivering it to *prp1* mutants, though this required higher doses of MO than we used previously (22) so that a MO-induced phenotype could be observed (in our hands, disruptions to gastrulation are very rare with these MO reagents, but other morphological defects are apparent, see Supplemental Figure S13). High dose *prp1* MO did not have any less impact on *prp1* mutants compared to wild type embryos (Supplemental Figure S13). Thus this test does not support *prp1* MO specificity at high MO doses. Testing MO specificity in this fashion at low *prp1* MO dosage is precluded by lack of phenotypes produced, therefore the thorough tests reviewed above remain as the best available evidence and strongly support *prp1* MO specificity at the low doses previously used (22).

In this instance, one reasonable interpretation of the data is that the mutagenesis and morpholino approaches towards disrupting *prp1* both have good efficacy and specificity, at least at some doses, despite producing disparate results (see below). On the other hand, both

approaches present with sufficient complexity that it is not possible to draw final conclusions. Our interpretations of these phenotypes, with respect to the role of PrP^C in development and in healthy brains, thus intentionally avoids contrasting mutant *vs*. morphant data sets and centers instead on the phenotypes that were found to be in common during disparate disruptions of PrP^C homologs in zebrafish. Going forward, and in consideration of this complexity, we do not expect to use morpholino reagents to address questions regarding PrP^C loss-of-function.

Moving beyond the putative technical intricacies discussed above, there may also be more fundamental (more biologically interesting) reasons why prion loss-of-function phenotypes would differ between techniques. For context, it is worth considering how varied the phenotypes have been amongst the various *Prnp* knockout mice (60), so some variation in outcomes when we are instead applying distinct methods of gene disruption might not be surprising. Beyond such (un)expected variations, it is notable that morpholino knockdown *acutely* exposes the larvae to loss of prion protein function; this contrasts the mutagenesis or prion knockout approaches, wherein gene compensation is likely: Mutagenesis and breeding towards homozygosity has an unavoidable consequence of selecting for individuals that can survive (and thrive to breeding age) with disrupted prion protein (e.g. consider the multiple generations of heterozygous animals that preceded the homozygous animals characterized herein; consider that homozygous animals failing to compensate may never successfully develop). Thus gene compensation is reasonably likely, and individuals with prion genes mutated or knocked out likely have compensatory alterations in other gene products in the prion network. Indeed an interesting parallel was observed following disruption of *Shadoo* ("shadow of prion protein", *Sprn,* a closely related family member of PrP^C) in mice: Acute loss of Shadoo by lentiviral delivery of sh-RNA led to lethality, and this was dependant upon a *Prnp* KO background, whereas Shadoo knockout mice reveal no overt phenotypes even when combined with *Prnp* KO (61-63). Thus in both mice and zebrafish loss of prion gene paralogs by acute methods leads to embryonic lethality, whereas stable mutation or knockout produces only subtle phenotypes. One approach to reconcile the disparate impacts following acute loss versus long-term loss of PrP^C would be via conditional ablation such as in the Cre-Lox system. In this strategy, fish or mice with floxed *Prnp* alleles would not be expected to experience any *Prnp* loss-of-function (or undergo selection pressure due to loss of PrP^C function) prior to being bred into animals with a Cre-driver line. This would allow acute disruption (though maybe not complete loss) of these proteins while avoiding the eccentricities of gene knockdown and the selection pressure leading to compensation inherent in gene knockout. Conditional knockout of mouse *Prnp* has indeed produced intriguing results (64), however we are not aware of this experiment being done using a driver line with the broad Cre expression as our experimental design would demand (reviewed in (2)).

In the meantime, we have generated zebrafish loss-of-function *Prnp* mutants that can now be used to interrogate the normal molecular and physiological functions of PrP^C. Several of these intriguing functions may be partially lost or subverted during prion diseases and Alzheimer's disease.

The zebrafish genome contains a third gene that was annotated as a prion protein gene due to some recognizable motifs in a similar gene in *Fugu* (15,65), though this was prior to a reliable genome assembly and the identification of *prp1* or *prp2*; however this gene ("*prnpa"* or "*PrP3*", ZFIN ID: ZDB-GENE-041217-6) is not an obvious paralog of *prp1* or *prp2*, and is not apparently present in the genomes of animals beyond some fishes. The predicted gene product lacks the critical domains and organization that would assign it even as a member of related doppel or shadoo protein families, or in the broader ZIP family from which PrP^C evolved. Thus as noted during its original description, *prnpa* is not recognizable to a prion biologist due to structural inconsistencies (65), and while it may indeed emerge to be of interest elsewhere, it is not expected that it will contribute to understanding prion biology and therefore is not considered further here.

The phenotypes observed in our prion mutants include marginally reduced larval size, disruptions to neurodevelopment revealed in the lateral line, and susceptibility to seizures. We discuss the latter two topics below, and broadly

note that in all three of these phenotypes it was observed that the coordinate loss of both *prp1* and *prp2* either reduced or blunted the phenotypes compared to losing either gene alone: this demonstrates that the prion gene paralogs are *not* redundant in (several of) their function(s) as we had predicted. The apparent oppositional actions of the paralogs inspires some speculations about their roles, which remain untested but are introduced below.

Prion proteins contribute to cell cohesion during neurodevelopment, as revealed by neuromast patterning within the zebrafish PLL—Upon finding that *prp1*$^{-/-}$ mutants and compound *prp1*$^{-/-}$*;prp2*$^{-/-}$ fish have no overt phenotypes, we went on to use these fish to study the role of PrP^{C} in neural development. We hypothesized that the zebrafish *prp1* and *prp2* would have redundant functions in posterior lateral line (PLL) development. We found that both *prp1* and *prp2* contributed to neuromast patterning, but they appeared to have opposing roles: loss of prp1 (in *prp1*$^{-/-}$ mutants) led to a reduced number of neuromasts, consistent with the phenotype previously observed in *prp2* morphants (30), while loss of Prp2 in (in *prp2*$^{-/-}$ mutants) led to an increase in neuromast number and premature deposition of the L1 neuromast. These results countered our expectation that *prp1* and *prp2* would be redundant in development of the PLL such that their concerted disruption would exacerbate the observed phenotypes.

Hypothetical mechanisms underlying abnormal neuromast patterning in zebrafish PrP mutants—We speculate that zebrafish *prp1* or *prp2* loss-of-function could interfere with neuromast formation/deposition at multiple levels. First, loss of Prp1 function could reduce neuromast number at the level of Wnt/β-catenin-signaling. Inhibition of β-catenin has been found to reduce the number of proneuromasts in the developing lateral line primordium (66). GSK-3β phosphorylates cytosolic β-catenin, inducing its destruction by the proteasome (reviewed in (67)). As PrP^{C} has been shown to inactivate GSK-3β through caveolin/Lyn (68), reduction in neuromast number in *prp1*$^{-/-}$ mutants could be due to increased degradation of β-catenin and subsequent reduction in β-catenin signaling. Further, loss of Prp2 function could increase neuromast number and cause premature deposition of the L1 neuromast by disrupting Notch signaling. Notch signaling normally restricts hair cell progenitor formation (69). In part this is because *atoh1a*, expressed by hair cells, restricts E-cadherin expression (69). Therefore it is possible that *prp2* loss-of-function causes an increase in neuromast number by impacting the Notch pathway. Finally, differential localization and/or levels of cell adhesion molecules in *prp1*$^{-/-}$ and *prp2*$^{-/-}$ mutants may influence proneuromast rosette cohesion (and hence neuromast number and patterning). E-cadherin is one candidate cell adhesion protein that may be mislocalized in *prp1*$^{-/-}$ and/or *prp2*$^{-/-}$ mutants. PrP^{C} downregulation has been shown to contribute to abnormal adherens junctions in Human A431 epidermoid carcinoma cells (70). The authors proposed that PrP^{C} participates in activating Src kinases that in turn reduce macropinocytosis of E-cadherin from adherens junctions by promoting EGFR endocytosis (70). Testing these hypotheses within the zebrafish PLL will provide further insight into the functions of PrP^{C}.

Prion protein has an ancient and conserved role in regulating neural activity—PrP^{C} is linked to several neuroprotective functions, though the molecular mechanisms typically remain to be revealed. One such case is a role for PrP^{C} in regulating neural excitability, perhaps on a continuum towards excitotoxicity, such that lack of PrP^{C} leads to disruptions of various channel physiologies and seizure susceptibility. Intriguingly, seizures occur in a subset of patients with prion and Alzheimer disease, which might coordinate with a loss of PrP^{C} function (40-43). Observations in *Prnp* knockout mice have revealed a seizure susceptibility phenotype, and controversy surrounding this topic appears to be partially reconciled by considering differences in how the knockout mice were engineered (38,39). Further, data from zebrafish *prp2* mutants supported a role for PrP^{C} in regulating seizures in an independent system (16). Intriguingly, this also implies that the PrP^{C} in the last common ancestor of fish and mammals had a role in regulating neural excitability. Indeed that notion was partially supported by examining the impacts of PrP^{C} loss on NMDA Receptors, wherein the kinetics of channel closing were pushed towards hyperexcitability in both fish and mice (16). Further roles for PrP^{C} at the synapse appear to be

shared between mice and zebrafish, because its loss in either species leads to deficits in learning and memory (27,71).

It is therefore of substantial interest to appreciate if other divergent PrP^C variants may impact upon seizure susceptibility. Broadly, our characterization of increased seizure susceptibility in *prp1*$^{-/-}$ mutant zebrafish confirms this in a second fish paralog, and adds good support to the notion that an ancient PrP^C had some role in regulating neurophysiology.

Intriguingly, loss of *prp1* did not exacerbate the similar seizure susceptibility phenotype we documented for *prp2* mutants. Indeed we had predicted the impacts would be additive or synergistic, such that compound mutants would present with more dramatic responses to convulsants. Our data clearly rejects this, and the loss of *prp1* significantly blunted the seizure susceptibility of *prp2* mutant fish. This suggests that the impacts of *prp1* and *prp2*, though producing similar outcomes, are occurring through disparate mechanisms. Future work should focus on comparing and contrasting these mechanisms, as they have potential to reveal the nuances of how PrP^C impacts upon neurophysiology, including excitotoxicity, learning and memory. It may be that future work documenting differences in the PrP^C paralogs' structures would lead to novel hypotheses. Some speculation about such mechanisms are detailed below, in hopes they suggest some new experimental designs.

Hypothetical mechanisms to explain the apparent rescue of developmental phenotypes and hyperactivity in compound prp1$^{-/-}$*;prp2*$^{-/-}$ *compound mutants*—One alternative hypothesis to explain the apparent rescue of neuromast patterning in compound *prp1*$^{-/-}$*;prp2*$^{-/-}$ mutants is that Prp1 and Prp2 act at different stages of development (e.g. have sub-functionalized roles in neuromast patterning), and a disruption in one phase of development is countered by a second disruption later in development. An example was discussed above – it may be that loss of prp1 may cause a partial reduction in Wnt/β-catenin signaling leading to an initial reduction in the number of proneuromast rosettes in the primordium. Later, however, loss of Prp2 function may reduce Delta/Notch lateral inhibition producing an extra hair cell progenitor (and eventually an extra proneuromast rosette).

An alternative explanation that could account for the apparent rescue of phenotypes observed in single mutants (neuromast patterning defects, body size and hyperactivity) in compound *prp1*$^{-/-}$*;prp2*$^{-/-}$ mutants is that the gene paralogs have evolved antagonistic roles (e.g. see schema in Supplemental Figure S6). Antagonistic roles have been observed for other gene paralog pairs. For example, in zebrafish ribosomal protein L22 (Rpl22) represses SmadI expression and hematopoietic stem cell emergence, while its paralog ribosomal protein L22 like1 (Rpl22l1) activates SmadI expression and hematopoietic stem cell emergence (72). Further, in mammals it has been found that Regulator of nonsense transcripts 3B (UPF3B) activates Nonsense-mediated decay through its interaction with the Exon-junction complex (EJC). In contrast, EPF3A acts as a repressor of nonsense mediated decay due to its weaker interaction with EJC. Hence, gene paralogs may develop antagonistic roles of the parent gene due to disruption of an important functional domain (73). Therefore, it is possible that loss of *prp1* dampens sensitivity to convulsant in *prp2*$^{-/-}$ larvae because Prp1 and Prp2 have an antagonistic effect on a common pathway. Further, it is possible that *prp2* cannot replace *prp1* in regulating larval size because Prp2 cannot effectively interact with a protein that Prp1 normally interacts with. In single mutants, the remaining *prp* paralog outcompetes with a third protein for a place in the relevant protein complex. However, in double *prp* mutants this third protein would be expected to be able to compensate for loss of the active *prp* paralog. It remains to be determined what protein(s) might be at the centre of this putative antagonism, though candidates may include molecules such as mGluR5 and APP that are thought to transduce extracellular signals bound to PrP^C through to the intracellular compartment (2,8,22,74,75). Identifying commonalities and differences amongst the functions of zebrafish *prp1*, *prp2* and mammalian *Prnp* is expected to inspire new hypotheses about the key functions of PrP^C and their relevance to the aetiology of neurodegeneration.

Conclusions—In summary, we have generated new genetic resources to study the function of PrP^C in healthy organisms (zebrafish *prp1*$^{-/-}$ and compound *prp1*$^{-/-}$*;prp2*$^{-/-}$ mutants), through early development and in adulthood, and

demonstrated that zebrafish prion proteins participate in neuromast patterning and regulating neurophysiology. As such, loss of functional PrP^C during prion and Alzheimer's disease may impair adult neurogenesis, neuron survival, or contribute to producing disease symptoms such as memory loss. Further study of the mechanisms through which prion proteins contribute to neuromast patterning and neurophysiology in the zebrafish will provide new insights into PrP^C's role in neural development and maintenance. Considering the disruption/subversion of PrP^C's function in both prion disease and Alzheimers disease (for review see (1,2)) these studies will likely uncover putative therapeutic targets for prion diseases and Alzheimer's disease.

EXPERIMENTAL PROCEDURES

Animal ethics and zebrafish husbandry—Zebrafish were raised and maintained using protocols approved by the Animal Care & Use Committee: Biosciences at the University of Alberta, operating under the guidelines of the Canadian Council of Animal Care. The fish were raised and maintained within the University of Alberta fish facility at 28°C under a 14/10 light/dark cycle as previously described (76).

Fish lines/strains—Zebrafish of the AB strain were used as the wild type fish in this study and were the background strain for the targetted mutagenesis. Our previously published *prp2*^{ua5001} allele (ZFin ID: ZDB-ALT-130724-2), which has a 4 base pair deletion and is predicted to produce a truncated protein lacking all recognizable protein domains (16), was maintained on an AB background. Tg(*cldnb:gfp*) larvae (Tg *(-8.0cldnb:Ly-EGFP*, ZFin ID: ZDB-ALT-060919-2; referred to herein as *cldnb:gfp* (37) were kindly provided by Pierre Drapeau and were bred into fish with the newly generated *prp1 ua5004* allele upon reaching adulthood.

Targetted mutagenesis—Targetted mutagenesis was performed on the zebrafish *prp1* gene (Ensemble ENSDARG00000044048, ZFIN ZDB-GENE-041221-2) using TALENs. The target sequence within the *prp1* genes is shown in Supplementary Figure S3A, and a flowchart summarizing the steps involved in the targetted mutagenesis process is shown in Supplementary Figure S3B. The location of the target sequence within the *prp1* gene is schematized in Figure 1.

Targetted mutagenesis: Production of TALEN plasmids—Custom TAL blocks™ and heterodimeric backbone plasmids were ordered from Transposagen (Lexington, KY, USA; http://www.transposagenbio.com). The backbone contains the first half site of the DNA binding domain, the sequence that recognizes the final base of the target site, and the FokI cleavage domain. The TAL blocks, which contain the remainder of the DNA binding domain, were assembled via Transposagen's FLASH build process. After digestion with BsmBI (NEB catalogue #R0580S, Ipswich, MA, USA), the vectors were purified using an Agencourt AMPure XP - PCR Purification kit (Beckman Coulter catalogue #A63880, Indianapolis, IN, USA). The custom TAL blocks™ of the forward TALEN were then ligated into the appropriate vectors (JDS 82 KKR heterodimer with NN to recognize the final cytosine in the *prp1* target sequence) with T4 ligase (Invitrogen/ Thermo Fisher Scientific catalogue #15224-017, Waltham, MA, USA) and transformed into Stbl3 cells (Invitrogen/Thermo Fisher Scientific catalogue #C7373-03, Waltham, MA, USA). Due to changes in Transposagen's manufacturing process, the *prp1* reverse TAL block™ was provided by Transposagen as pre-ligated plasmids. Colony PCR was performed to screen for colonies with the correct number of repeats (Supplementary Figure S4), and those yielding PCR products of the appropriate length were sequenced to ensure that they contained the correct TALEN sequence (see Supplementary Table S1 for primer sequences; sequencing performed by the University of Alberta's Molecular Biology Service Unit). Clones with the full TALEN sequence were then prepared using a Plasmid Maxiprep kit (Qiagen catalogue #12163, Toronto, ON, Canada).

Targetted mutagenesis: Production of TALEN mRNA and its delivery to zebrafish embryos—mRNA was synthesized from maxi-prepped plasmid DNA that had been linearized with Fast digest MssI (Thermo Fisher Scientific catalogue #FD1344, Waltham, MA, USA) and purified by ethanol precipitation. Briefly, 1 uL of 0.5 M EDTA pH 8, 2 uL 3M sodium acetate and 40 uL of 100% ethanol were added to the linearized plasmid and frozen overnight at -80°C. Linearized plasmid was then centrifuged for 15 minutes at 13 000 RPM at 4°C and the supernatant

was removed. The pellet was then suspended in 6 µL of nuclease free water. mRNA was synthesized using the mMESSAGE mMachine T7 Ultra Kit (Invitrogen/Thermo Fisher Scientific catalogue #AM1345, Waltham, MA, USA) including the polyA tailing reaction as per manufacture's protocol. 100 pg each of *prp1* forward and reverse TALENs were injected into AB strain wild type zebrafish embryos. 25 pg of *egfp* mRNA was co-injected with the TALEN mRNA so that fish that were successfully injected could be identified and raised to adulthood. *egfp* mRNA was produced from pCS2+*egfp* by first linearizing the plasmid with Fast digest NotI (Thermo Fisher Scientific catalogue #FD0593, Waltham, MA, USA) and then transcribing mRNA using the mMESSAGE MMachine SP6 Kit (Invitrogen/Thermo Fisher Scientific catalogue #AM1340, Waltham, MA, USA).

Targetted mutagenesis: Detection of larvae with somatic and germline mutations in prp1—The first step in our analyses of TALEN-effectiveness was determining whether TALENs induced somatic mutations in injected embryos (F0 generation). Siblings of successfully mutated F0 fish were grown to adulthood. F0 fish were then bred and pools of F1 generation embryos were screened for successful germline transmission of TALEN-induced mutations. For detection of both somatic and germline-transmitted mutations in embryos, genomic DNA was isolated from pools of test fish (injected F0 embryos for detection of somatic mutations, or offspring of F0 embryos for detection of germline-transmitted mutations) or un-injected wild type AB strain fish at either 24 hpf or 3 dpf using a protocol modified from (77). Briefly, samples (pools of up to 20 embryos) were boiled for 15 minutes in 50 mM NaOH (5 uL/embryo), cooled on ice for 5 minutes and neutralized with 1 M Tris-HCl,pH 8 (0.5 uL/embryo). Genomic DNA was then diluted tenfold in sterile Milli-Q water prior to High Resolution Melt (HRM) analysis. Diluted genomic DNA was amplified using HRM primers (Supplementary Table S2) and MeltDoctor™ HRM Master Mix (Thermo Fisher Scientific catalogue #4415440, Waltham, MA, USA). HRM data was generated using the Applied Biosystems 7500 Fast Real-Time PCR System with MeltDoctor™ HRM Master Mix. Data was then analyzed using the High ReSolution Melt (HRM) Software (Version 2.0, High ReSolution Melt, Thermo Fisher Scientific, Waltham, MA, USA).

Upon identification of pools of genomic DNA with distinct melt profiles compared to un-injected wild type AB strain samples, those pools (and wild type control pools) were PCR-amplified with amplicon primers (Supplementary Table S2) and cloned into the pCR2.1 Topo vector as per the instructions in the TOPO TA cloning kit (Invitrogen/Thermo Fisher Scientific catalogue #K4500-01, Waltham, MA, USA). Clones were dissolved in 25µL sterile Milli-Q water for HRM analysis, and a portion of each clone was streaked on agar plates for subsequent analysis. Clones with a different melt profile compared to control clones were mini-prepped with a Qiaprep Spin Miniprep Kit (Qiagen catalogue #27106, Toronto, ON, Canada) and submitted to the U of A's Molecular Biology Service Unit for sequencing.

Targetted mutagenesis: Identification of adult F1 generation fish that are heterozygous for TALEN-induced mutations in prp1—Siblings of F1 embryos that had germline transmitted TALEN mutations were grown to adulthood. These adult F1 fish were then screened to identify carriers of TALEN mutations. Fish were anaesthetized with 4.1% tricaine and a small piece of caudal fin was harvested. Genomic DNA extraction was performed as above, but with 15 uL of 50 mM NaOH and 1.5 uL Tris-HCl per sample. DNA was diluted either twenty-fold or thirty-fold in sterile Milli-Q water prior to HRM analysis. A PCR product (primers shown in Supplementary Table S2) containing the target site was amplified from genomic DNA and was cloned into the pCR2.1 Topo vector using a TOPO TA cloning kit (Invitrogen/ Thermo Fisher Scientific catalogue #K4500-01, Waltham, MA, USA). The construct was then mini-prepped with a Qiaprep Spin Miniprep kit (Qiagen catalogue #27106, Toronto, ON, Canada) and sequenced using a T7 primer sequence within the vector (5'-TAA TAC GAC TCA CTA TAG GG-3').

Genotyping: HRM to identify fish with mutant prp1 alleles—Once stably inherited alleles had been identified (see Methods and Results), methods were developed for genotyping individual fish. Genomic DNA was amplified using HRM as described above. Sample melt curves are shown in Supplementary Figure S5. One round of HRM

(Primers listed in Supplementary Table S2) was used to distinguish the genotype of fish for the *prp1 ua5004* allele. The accuracy of this method was confirmed by sequencing the area around the target site. Briefly, a 453 base pair region around the target site was amplified (Primers in Supplementary Table S2). The amplicon was either cloned into pCR2.1, followed by sequencing of mini-prepped plasmid with a T7 vector specific primer (5'-TAA TAC GAC TCA CTA TAG GG-3') or the PCR-product was treated with Illustra ExoProstar (Sigma catalogue #US78210, St. Louis, MO, USA) as specified in the manufacturer's instructions, and directly sequenced using the same primers used to generate the amplicon. HRM to screen for $prp1^{+/ua5003}$ and $prp1^{ua5003/ua5003}$ fish was performed in a two-step process because genomic DNA from wild type and $prp1^{ua5003/ua5003}$ fish had overlapping melt profiles (See Supplemental Figure 5A). Thus heterozygous individuals could be discriminated from homozygous individuals, but homozygous fish were not clearly mutant or wild type. In the second round of HRM, 0.5 uL of sample genomic DNA was spiked with 0.5 uL of known DNA (wild type or homozygous mutant) and diluted twenty-fold in sterile Milli-Q water. The accuracy of this method was confirmed by sequencing as described above for the *ua5004* allele.

Genotyping: RFLP to detect fish heterozygous and homozygous for the ua5001 allele—For ease of genotyping fish with the $prp2^{ua5001}$ allele previously isolated (16), a Restriction Fragment Length Polymorphism (RFLP) assay was developed, as reported recently (27). Genomic DNA was amplified using *prp2* RFLP primers (Supplementary Table S2), and then digested with Fast Digest Mva I (Thermo Fisher Scientific, catalogue #FD0554, Waltham, MA, USA). As the ua5001 mutation disrupted the Mva I cut site, PCR products from mutant and wild type DNA produced different banding patterns on an Ethidium bromide agarose gel (wild type allele yields 3 bands with sizes of 21, 36 and 54 base pairs; ua5001 allele yields 2 bands with sizes of 36 and 71 base pairs; Supplementary Figure S5C). The accuracy of this genotyping assay was confirmed by sequencing. Briefly, a 1039 base pair region around the target site was amplified (Primers in Supplementary Table S2), and sequenced using the same primers used to generate the amplicon after treatment with Illustra ExoProstar (Sigma catalogue #US78210, St. Louis, MO, USA) to remove unincorporated nucleotides.

RT-qPCR to quantify prp1, prp2 or cfos transcripts abundance—Experiments were performed in compliance with the MIQE guidelines (Minimum Information for Publication of Quantitative Real-Time PCR Experiments) (78). RNA samples for comparing *prp1* and/or *prp2* transcript abundance were obtained from pools of larvae at the ages noted (each biological replicate represents 15-20 larvae) that had been stored in RNAlater (Ambion/Thermo Fisher Scientific, catalogue #AM7021, Waltham, MA, USA). RNA samples for comparing *prp1* transcript abundance in $prp1^{ua5004/ua5004}$ mutants versus *prp1* transcript abundance in wild type fish were obtained from pools of 2dpf larvae (each biological replicate represents 5 larvae) and stored in RNAlater. Total RNA was extracted from pools of embryos using the RNeasy Kit (Qiagen catalogue #74104,Toronto, ON, Canada) as outlined in the manufacturer's protocols. The samples were homogenized in the appropriate lysis buffer (Buffer RLT for larvae) with a rotor stator homogenizer (VWR catalogue #47747-370, Radnor, PA, USA), and on-column DNA digestion was performed using Qiagen DNase I (Qiagen catalogue #79254, Toronto, ON, Canada). RNA quantity was determined using a Nanodrop 2000 spectrophotometer (Thermo Scientific). All of the samples had ribosomal RNA profiles with strong 28S and 18S bands and RNA integrity numbers of at least 7/10 as determined using an Agilent RNA 6000 NanoChip and Agilent 2100 Bioanalyzer. cDNA was then generated using a qScript Supermix kit (Quanta BioSciences catalogue #95048-100, Beverly, MA, USA).

Quantitative PCR (qPCR) was performed using a 7500 Real-Time PCR system (ABI Applied Biosystems). Primers were designed using Primer Express (Version 3.0, Primer Express, Thermo Fisher Scientific, Waltham, MA, USA) and the *prp1*, *prp2* and *β-actin* primers were previously verified with standard curves and melt curves (16). These primers were further verified here by confirming that no product was apparent when reverse transcriptase was left out of the cDNA synthesis. The *c-fos* qPCR primers (forward: 5'-GCAAAGACCTCCAACAAGAGA-3'; reverse:

5'- TTTCGCAGCAGCCATCTT-3') span intron 2-3 of the *c-fos* gene (PMID Gene ID:394198; ZFIN ID: ZDB-GENE-031222-4) and produce a 102 bp product from cDNA. qPCR reactions were performed with 3 technical replicates of each biological replicate. Each reaction contained 5 µL Dynamite Master Mix (prepared and supplied by Molecular Biology Service Unit, University of Alberta. The mix included SYBR Green and platinum Taq hot start enzyme), 2.5 µL of pre-mixed primer working stocks (final concentrations of the *β-actin*, *c-fos* and *prp1* primers were 800 nM, 800 nM and 200 nM, respectively) and 2.5 µL cDNA for a total volume of 10 µL. After an initial denaturation step (2 min at 95 °C), cycling consisted of 40 cycles of 95 °C for 15 s followed by 60 °C for 1 min. One cycle for melting dissociation curve analysis followed these 40 cycles and consisted of 95 °C for 15 s, 60 °C for 1 min, 95 °C for 15 s, and finally 60 °C for 1 min. Data analysis was performed using 7500 Software for 7500 and 7500 Fast Real Time PCR Systems version 2.0.1 (AB Applied Biosystems) with auto Ct calling. Transcript abundance was normalized to *β-actin* levels. Relative fold change in transcript abundance was statistically analyzed on the resulting RQ values.

Characterizing mutant transcripts—To assess if *prp1* and *prp2* transcripts had the expected length and content, RACE (Rapid Amplification of cDNA Ends) was performed as per the kit instructions (Clontech catalogue #634860, Fremont CA) using mRNA isolated as per RT-qPCR methods above. 5'RACE used gene-specific primers reported in Supplementary Table S3. Transcript lengths were compared between mutant and wild type by gel electrophoresis and validated by sequencing. Transcripts were also characterized by examining the alignment of RNA-Seq reads around both the *prp1* and *prp2* genes by comparing 3 dpf wildtype and *prp1*$^{-/-}$*;prp2*$^{-/-}$ larvae. Pools of 50 larvae from each genotype were homogenized in Trizol (Invitrogen/ Thermo Fisher Scientific catalogue # 15596026) and shipped to Otogenetics (Atlanta GA) for Illumina RNA-sequencing, and DNAnexus Platform standard RNAseq analysis at a depth of >41M reads each.

Measuring the length of larval zebrafish—2 dpf larvae were fixed overnight in 4% paraformaldehyde (PFA) in phosphate buffer (pH 7.4) with 5% sucrose at 4°C. Larvae were then rinsed several times with 1xPBS and imaged and photographed with a Leica M165 FC dissecting microscope and a Leica DFC 400 camera. The scale bar feature in the Leica software was then used to measure the length of each fish from the forebrain to the tip of the caudal fin.

Alkaline Phosphatase staining—Neuromasts are rich in endogenous alkaline phosphatase and staining for this allows for their observation. Zebrafish larvae were fixed in 4% paraformaldehyde (PFA) in phosphate buffer (pH 7.4) with 5% sucrose for 3–3.5 hours at room temperature. They were subsequently washed 4x in phosphate buffered saline (PBS; pH 7.4) with 0.1% tween (PBST) and then for 15 minutes in fresh alkaline phosphatase buffer (pH 9.5; 100 mM Tris-HCl, 100 mM NaCl, 50 mM MgCl2) with 0.1% tween. They were developed in alkaline phosphatase buffer containing 0.225% NBT and 0.175% BCIP (Roche catalogue #s11383213001 and 11383221001, Basel, Switzerland) for approximately 10 minutes. Fish were then washed for 30 minutes in alkaline phosphatase wash buffer (pH 7.5;154 mM NaCl, 11 mM Tris/ HCl, 1 mM EDTA) with 0.1% tween, fixed in 4% PFA with 5% sucrose, and washed 3x in PBST. Some fish were counterstained with Phalloidin 488 or 555 (Invitrogen Molecular Probes, catalogue #sA12379 and A34055, Eugene OR, USA) prior to imaging. For this, fish were incubated in PBS with 2% Triton X100 for 2 hrs. Phalloidin 488 was diluted twenty-fold in PBS with 2% Triton X 100 and left overnight at 4°C. Fish were then washed 3x 20 minutes in PBS with 2% triton and then washed into PBS with 0.1% tween. Wholemounts were transferred to a PBST/glycerol mixture and imaged with a Leica M165 FC dissecting microscope and Leica DFC 400 camera.

Analysis of neuromast number and position—Trunk neuromasts of the PLL were visualized by alkaline phosphatase NBT/BCIP staining as described above, or by detection of GFP fluorescence in *Tg*(*cldnb:gfp*) using a Leica M165 FC dissecting microscope. An observer, who was blinded to the genotype of the fish, counted the number of neuromasts. In some analyses, we examined neuromast number with respect to somite number. In some 3 dpf larvae we noticed lighter stained neuromasts between the L1 and L2 neuromasts. These were likely neuromasts

of the secondary posterior lateral line system (see Figure 4). We considered these to be part of the secondary posterior lateral line system, and excluded them from our counts if they were ≤ 5 somite lengths posterior to the L1 neuromasts.

Locomotor activity measurements of PTZ-induced seizures—Assays for measuring stage I and II seizures were performed according to established methods (79,80), and behavioral tracking software was used to quantify the activity and velocity of zebrafish larvae arrayed in 96-well plates. Larvae at age 4 dpf were carefully pipetted into 96-well plate (7701-1651; Whatman, Clifton, NJ) containing 650 µl of their typical embryonic growth media (E3 media) and were acclimatized for 3 h prior to baseline recording for 1 h. This was followed by treatment with various doses of PTZ (2.5 – 15.0 mM) for 2 h. Plates were placed on top of an infrared backlight source and below a Basler GenICaM (Basler acA 1300-60) scanning camera, both provided by Noldus (Wageningen, Netherlands), which were used to track locomotor activity of an individual larvae within each well. EthoVision® XT-11.5 software (Noldus) was used to quantify locomotor activity, which was defined as % pixel change within a corresponding well between samples (motion was captured by taking 25 samples (frames) per second), similar to described previously (81). Thus the absolute numbers recorded can appear to be small, as only a small percentage of pixels in the region of interest (a well in a 96-well plate) might be changing at any one time and bursts of activity may occur such that total movement is small within any given minute. Thus the absolute values are not especially meaningful in these assays, which operationally are both sensitive and robust insomuch that the data is reproducible between trials and gives rational outcomes in dose-response formats. The results are consistent with those attained when the same behavioural traces were assessed for their mean velocity (Supplemental Figure S7). For baseline activity (Figure 5D) and PTZ time-course experiments (Figure 5B) data was calculated directly, whereas for PTZ dose-response (Figure 5C) mean activity following 30 min PTZ treatment was normalized to 1 h baseline activity prior PTZ addition. All data reported from mutant larvae herein are from maternal zygotic larvae.

Further analysis of seizure behaviour (in Supplemental Figure S9) used different optics on the camera (a 75 mm f2.8 C-mount lens, Noldus) that improved fidelity of larval tracking, allowed assessment of further parameters, and permitted use of 96 well plates with round wells (Costar #3599). Larvae were kept in 100 µl E3 media and tracked with daniovision software. To exclude background noise, active movement was defined as >0.2mm at >2mm/sec velocity. Outliers were removed objectively using ROUT Q=0.1 for velocity, number of movements, and movement duration. For activity, Q was set to 10, but only 3 outliers were detected in wild type.

Detecting c-fos by in situ hybridization—Probe production: RNA was extracted from wild type zebrafish larvae using an RNeasy Mini Kit (Qiagen catalogue #74104, Toronto, ON, Canada). A 602 base pair cDNA product was then produced from wild type zebrafish larvae using a Qiagen LongRange 2-Step RT-PCR kit (Qiagen catalogue #205920, Toronto, ON, Canada). For the initial PCR reaction, primers from a previous publication were used: Forward: 5'-TCTCCTCTGTGGCGCCCTCC-3'; Reverse 5'GTCTGGAACCGAGCGAGCCG-3' (82). The cDNA product was then cloned into the pCr2.1 Topo vector (Invitrogen) and sequenced to verify the insert orientation in the plasmids. The resulting plasmid was linearized with FastDigest KpnI (ThermoFisher Scientific catalogue #FD0524, Waltham, MA, USA) and used to template production of DIG-labeled riboprobe with T7 RNA polymerase (Roche/Sigma catalogue #10881775001, St. Louis, MO, USA). After PTZ or vehicle treatment, fish were rinsed with E3 medium and fixed overnight in 4% (PFA) in phosphate buffer (pH 7.4) with 5% sucrose. Fish were then washed in 50% methanol/DEPC-treated water for 5 minutes, rinsed in 100% MeOH and stored at least overnight in 100% MeOH at -20° C. In situ hybridization was performed as previously described (16), except that the hybridization temperature was 60° C.

Statistical Analysis—All statistics were performed using GraphPad Prism Software (Version 6, GraphPad, San Diego, CA). Prior to performing pairwise comparisons between groups, the F-test was used to assess variance. If variance within groups was not statistically significant, pairwise comparisons were performed using paired t-tests. If variance was statistically different, Mann-Whitney *U* tests were performed

instead. For multiple group comparisons, groups were assessed for variance and normal distribution using the Brown Forsythe and Bartlett's tests. If variance was not significant, data was analyzed using One-Way ANOVAs, and if variance was significant, data was analyzed using a Kruskal Wallis test. RT-qPCR data was analyzed by performing statistics on the RQ values. For graphical presentation, data was normalized to the wild type samples and plotted as a percentage.

Statistical analysis of basal and seizure activity following exposure to convulsant used one-way ANOVA to compare basal activities across genotype and Dunnett's multiple comparison test. Two-way ANOVAs with Holm-Šídák multiple comparison test were used to compare the seizures across phenotypes and time, or across phenotypes and dose. Outlier data points were objectively removed, where indicated, using the ROUT function in the Prism software with Q=0.01.

Acknowledgements: We thank Laszlo Locksai, Jordyn Ko, Natasha Lifeso and Kirklin Maclise for technical assistance.

Conflict of interest: The authors declare that they have no conflicts of interest with the contents of this article.

Author contributions: PLAL and WTA designed and interpreted the experiments and wrote the paper. PLAL engineered the mutant zebrafish, and participated in and analyzed results from all experiments. RK performed and analyzed experiments shown in Figure 5 and related Supplemental Figures, and wrote the associated methods. NP provided technical assistance collecting data in Figure 4 and related Supplemental Figures, and in collecting tissues for RT-qPCR and RNA-Seq. GN provided technical assistance and analysis of genotyping, 5'RACE and RT-qPCR. WTA conceived of the experiments and was responsible for supervision and funding acquisition. All authors participated in animal husbandry, reviewed the results, edited the writing, and approved the final version of the manuscript.

REFERENCES

1. Leighton, P. L., and Allison, W. T. (2016) Protein Misfolding in Prion and Prion-Like Diseases: Reconsidering a Required Role for Protein Loss-of-Function. *J. Alzheimers Dis.* **54**, 3-29

2. Allison, W. T., DuVal, M. G., Nguyen-Phuoc, K., and Leighton, P. L. A. (2017) Reduced Abundance and Subverted Functions of Proteins in Prion-Like Diseases: Gained Functions Fascinate but Lost Functions Affect Aetiology. *Int J Mol Sci* **18**

3. Reimann, R. R., Sonati, T., Hornemann, S., Herrmann, U. S., Arand, M., Hawke, S., and Aguzzi, A. (2016) Differential Toxicity of Antibodies to the Prion Protein. *PLoS Pathog* **12**, e1005401

4. Lauren, J. (2014) Cellular prion protein as a therapeutic target in Alzheimer's disease. *J Alzheimers Dis* **38**, 227-244

5. Graner, E., Mercadante, A. F., Zanata, S. M., Forlenza, O. V., Cabral, A. L. B., Veiga, S. S., Juliano, M. A., Roesler, R., Walz, R., Minetti, A., Izquierdo, I., Martins, V. R., and Brentani, R. R. (2000) Cellular prion protein binds laminin and mediates neuritogenesis. *Molecular Brain Research* **76**, 85

6. Schmitt-Ulms, G., Legname, G., Baldwin, M. A., Ball, H. L., Bradon, N., Bosque, P. J., Crossin, K. L., Edelman, G. M., DeArmond, S. J., Cohen, F. E., and Prusiner, S. B. (2001) Binding of neural cell adhesion molecules (N-CAMs) to the cellular prion protein. *J. Mol. Biol.* **314**, 1209

7. Watts, J. C., Huo, H. R., Bai, Y., Ehsani, S., Won, A. H., Shi, T., Daude, N., Lau, A., Young, R., Xu, L., Carlson, G. A., Williams, D., Westaway, D., and Schmitt-Ulms, G. (2009) Interactome Analyses Identify Ties of PrPC and Its Mammalian Paralogs to Oligomannosidic N-Glycans and Endoplasmic Reticulum-Derived Chaperones. *PLoS Pathog.* **5**

8. Beraldo, F. H., Arantes, C. P., Santos, T. G., Machado, C. F., Roffe, M., Hajj, G. N., Lee, K. S., Magalhaes, A. C., Caetano, F. A., Mancini, G. L., Lopes, M. H., Americo, T. A., Magdesian, M. H., Ferguson, S. S., Linden, R., Prado, M. A., and Martins, V. R. (2011) Metabotropic glutamate receptors transduce signals for neurite outgrowth after binding of the prion protein to laminin gamma1 chain. *FASEB J* **25**, 265-279

9. Santuccione, A., Sytnyk, V., Leshchyns'ka, I., and Schachner, M. (2005) Prion protein recruits its neuronal receptor NCAM to lipid rafts to activate p59fyn and to enhance neurite outgrowth. *J Cell Biol* **169**, 341-354

10. Parrie, L. E., Crowell, J. A. E., Telling, G. C., and Bessen, R. A. (2018) The cellular prion protein promotes olfactory sensory neuron survival and axon targeting during adult neurogenesis. *Dev. Biol.* **438**, 23-32

11. Mehrabian, M., Brethour, D., Wang, H., Xi, Z., Rogaeva, E., and Schmitt-Ulms, G. (2015) The Prion Protein Controls Polysialylation of Neural Cell Adhesion Molecule 1 during Cellular Morphogenesis. *PLoS One* **10**, e0133741

12. Manson, J. C., Clarke, A. R., Hooper, M. L., Aitchison, L., McConnell, I., and Hope, J. (1994) 129/Ola mice carrying a null mutation in PrP that abolishes mRNA production are developmentally normal. *Mol Neurobiol* **8**, 121-127

13. Bueler, H., Fischer, M., Lang, Y., Bluethmann, H., Lipp, H. P., DeArmond, S. J., Prusiner, S. B., Aguet, M., and Weissmann, C. (1992) Normal development and behaviour of mice lacking the neuronal cell-surface PrP protein. *Nature* **356**, 577-582

14. Lieschke, G. J., and Currie, P. D. (2007) Animal models of human disease: zebrafish swim into view. *Nat Rev Genet* **8**, 353-367

15. Cotto, E., Andre, M., Forgue, J., Fleury, H. J., and Babin, P. J. (2005) Molecular characterization, phylogenetic relationships, and developmental expression patterns of prion genes in zebrafish (Danio rerio). *FEBS J* **272**, 500-513

16. Fleisch, V. C., Leighton, P. L., Wang, H., Pillay, L. M., Ritzel, R. G., Bhinder, G., Roy, B., Tierney, K. B., Ali, D. W., Waskiewicz, A. J., and Allison, W. T. (2013) Targeted mutation of the gene encoding prion protein in zebrafish reveals a conserved role in neuron excitability. *Neurobiol Dis* **55**, 11-25

17. Rivera-Milla, E., Oidtmann, B., Panagiotidis, C. H., Baier, M., Sklaviadis, T., Hoffmann, R., Zhou, Y., Solis, G. P., Stuermer, C. A., and Malaga-Trillo, E. (2006) Disparate evolution of prion protein domains and the distinct origin of Doppel- and prion-related loci revealed by fish-to-mammal comparisons. *FASEB J* **20**, 317-319

18. Malaga-Trillo, E., Solis, G. P., Schrock, Y., Geiss, C., Luncz, L., Thomanetz, V., and Stuermer, C. A. O. (2009) Regulation of Embryonic Cell Adhesion by the Prion Protein. *Plos Biology* **7**, 576-590

19. Malaga-Trillo, E., and Sempou, E. (2009) PrPs: Proteins with a purpose: Lessons from the zebrafish. *Prion* **3**, 129-133

20. Salta, E., Kanata, E., Ouzounis, C. A., Gilch, S., Schatzl, H., and Sklaviadis, T. (2014) Assessing proteinase K resistance of fish prion proteins in a scrapie-infected mouse neuroblastoma cell line. *Viruses* **6**, 4398-4421

21. Malaga-Trillo, E., Salta, E., Figueras, A., Panagiotidis, C., and Sklaviadis, T. (2011) Fish models in prion biology: underwater issues. *Biochim Biophys Acta* **1812**, 402-414

22. Kaiser, D., Acharya, M., Leighton, P., Wang, H., Daude, N., Wohlgemuth, S., Shi, B., and Allison, W. (2012) Amyloid beta precursor protein and prion protein have a conserved interaction affecting cell adhesion and CNS development. *PLoS One* **7**

23. Sempou, E., Biasini, E., Pinzon-Olejua, A., Harris, D. A., and Malaga-Trillo, E. (2016) Activation of zebrafish Src family kinases by the prion protein is an amyloid-beta-sensitive signal that prevents the endocytosis and degradation of E-cadherin/beta-catenin complexes in vivo. *Mol Neurodegener* **11**, 18

24. Miesbauer, M., Bamme, T., Riemer, C., Oidtmann, B., Winklhofer, K. F., Baier, M., and Tatzelt, J. (2006) Prion protein-related proteins from zebrafish are complex glycosylated and contain a glycosylphosphatidylinositol anchor. *Biochem Biophys Res Commun* **341**, 218-224

25. Bayes, A., Collins, M. O., Reig-Viader, R., Gou, G., Goulding, D., Izquierdo, A., Choudhary, J. S., Emes, R. D., and Grant, S. G. (2017) Evolution of complexity in the zebrafish synapse proteome. *Nat Commun* **8**, 14613

26. Singh, S., Ramamoorthy, K., Saradhi, A. P., and Idris, M. (2010) Proteome profile of zebrafish brain based on Gel LC-ESI MS/MS analysis. *J Proteomics Bioinform* **3**, 135-142

27. Leighton, P. L. A., Nadolski, N. J., Morrill, A., Hamilton, T. J., and Allison, W. T. An ancient conserved role for prion protein in learning and memory. LID - bio025734 [pii] LID - 10.1242/bio.025734 [doi].

28. Solis, G. P., Radon, Y., Sempou, E., Jechow, K., Stuermer, C. A., and Malaga-Trillo, E. (2013) Conserved roles of the prion protein domains on subcellular localization and cell-cell adhesion. *PLoS One* **8**, e70327

29. Nourizadeh-Lillabadi, R., Torgersen, J. S., Vestrheim, O., Konig, M., Alestrom, P., and Syed, M. (2010) Early Embryonic Gene Expression Profiling of Zebrafish Prion Protein (Prp2) Morphants. *PLoS One* **5**

30. Huc-Brandt, S., Hieu, N., Imberdis, T., Cubedo, N., Silhol, M., Leighton, P. L., Domaschke, T., Allison, W. T., Perrier, V., and Rossel, M. (2014) Zebrafish prion protein PrP2 controls collective migration process during lateral line sensory system development. *PLoS One* **9**, e113331

31. Culbertson, M. R. (1999) RNA surveillance. Unforeseen consequences for gene expression, inherited genetic disorders and cancer. *Trends Genet* **15**, 74-80

32. Pantera, B., Bini, C., Cirri, P., Paoli, P., Camici, G., Manao, G., and Caselli, A. (2009) PrPc activation induces neurite outgrowth and differentiation in PC12 cells: role for caveolin-1 in the signal transduction pathway. *J Neurochem* **110**, 194-207

33. Dambly-Chaudiere, C., Cubedo, N., and Ghysen, A. (2007) Control of cell migration in the development of the posterior lateral line: antagonistic interactions between the chemokine receptors CXCR4 and CXCR7/RDC1. *BMC Dev. Biol.* **7**, 23

34. Villablanca, E. J., Renucci, A., Sapede, D., Lec, V., Soubiran, F., Sandoval, P. C., Dambly-Chaudiere, C., Ghysen, A., and Allende, M. L. (2006) Control of cell migration in the zebrafish lateral line: implication of the gene "tumour-associated calcium signal transducer," tacstd. *Dev. Dyn.* **235**, 1578-1588

35. Ghysen, A., and Dambly-Chaudiere, C. (2007) The lateral line microcosmos. *Genes Dev* **21**, 2118-2130

36. Gompel, N., Cubedo, N., Thisse, C., Thisse, B., Dambly-Chaudiere, C., and Ghysen, A. (2001) Pattern formation in the lateral line of zebrafish. *Mech. Dev.* **105**, 69-77

37. Haas, P., and Gilmour, D. (2006) Chemokine signaling mediates self-organizing tissue migration in the zebrafish lateral line. *Dev. Cell* **10**, 673-680

38. Carulla, P., Llorens, F., Matamoros-Angles, A., Aguilar-Calvo, P., Espinosa, J. C., Gavin, R., Ferrer, I., Legname, G., Torres, J. M., and del Rio, J. A. (2015) Involvement of PrP(C) in kainate-induced excitotoxicity in several mouse strains. *Sci Rep* **5**, 11971

39. Striebel, J. F., Race, B., and Chesebro, B. (2013) Prion protein and susceptibility to kainate-induced seizures: genetic pitfalls in the use of PrP knockout mice. *Prion* **7**, 280-285

40. Vossel, K. A., Tartaglia, M. C., Nygaard, H. B., Zeman, A. Z., and Miller, B. L. (2017) Epileptic activity in Alzheimer's disease: causes and clinical relevance. *Lancet Neurol* **16**, 311-322

41. Ryan, N. S., Nicholas, J. M., Weston, P. S., Liang, Y., Lashley, T., Guerreiro, R., Adamson, G., Kenny, J., Beck, J., Chavez-Gutierrez, L., de Strooper, B., Revesz, T., Holton, J., Mead, S., Rossor, M. N., and Fox, N. C. (2016) Clinical phenotype and genetic associations in autosomal dominant familial Alzheimer's disease: a case series. *Lancet Neurol* **15**, 1326-1335

42. Wieser, H. G., Schindler, K., and Zumsteg, D. (2006) EEG in Creutzfeldt-Jakob disease. *Clin Neurophysiol* **117**, 935-951

43. Bertani, I., Iori, V., Trusel, M., Maroso, M., Foray, C., Mantovani, S., Tonini, R., Vezzani, A., and Chiesa, R. (2017) Inhibition of IL-1beta Signaling Normalizes NMDA-Dependent Neurotransmission and Reduces Seizure Susceptibility in a Mouse Model of Creutzfeldt-Jakob Disease. *J Neurosci* **37**, 10278-10289

44. Baraban, S. C., Taylor, M. R., Castro, P. A., and Baier, H. (2005) Pentylenetetrazole induced changes in zebrafish behavior, neural activity and c-fos expression. *Neuroscience* **131**, 759-768

45. Yu, G., Chen, J., Xu, Y., Zhu, C., Yu, H., Liu, S., Sha, H., Chen, J., Xu, X., Wu, Y., Zhang, A., Ma, J., and Cheng, G. (2009) Generation of goats lacking prion protein. *Mol. Reprod. Dev.* **76**, 3

46. Richt, J. A., Kasinathan, P., Hamir, A. N., Castilla, J., Sathiyaseelan, T., Vargas, F., Sathiyaseelan, J., Wu, H., Matsushita, H., Koster, J., Kato, S., Ishida, I., Soto, C., Robl, J. M., and Kuroiwa, Y. (2007) Production of cattle lacking prion protein. *Nat Biotechnol* **25**, 132-138

47. Benestad, S. L., Austbo, L., Tranulis, M. A., Espenes, A., and Olsaker, I. (2012) Healthy goats naturally devoid of prion protein. *Vet. Res.* **43**, 87

48. Malaga-Trillo, E., and Ochs, K. (2016) Uncontrolled SFK-mediated protein trafficking in prion and Alzheimer's disease. *Prion* **10**, 352-361

49. Ochs, K., and Malaga-Trillo, E. (2014) Common themes in PrP signaling: the Src remains the same. *Front Cell Dev Biol* **2**, 63

50. Schmitt-Ulms, G., Ehsani, S., Watts, J. C., Westaway, D., and Wille, H. (2009) Evolutionary descent of prion genes from the ZIP family of metal ion transporters. *PLoS One* **4**, e7208

51. Ehsani, S., Huo, H., Salehzadeh, A., Pocanschi, C. L., Watts, J. C., Wille, H., Westaway, D., Rogaeva, E., St George-Hyslop, P. H., and Schmitt-Ulms, G. (2011) Family reunion--the ZIP/prion gene family. *Prog Neurobiol* **93**, 405-420

52. Ehsani, S., Tao, R., Pocanschi, C. L., Ren, H., Harrison, P. M., and Schmitt-Ulms, G. (2011) Evidence for retrogene origins of the prion gene family. *PLoS One* **6**, e26800

53. Ehsani, S., Mehrabian, M., Pocanschi, C. L., and Schmitt-Ulms, G. (2012) The ZIP-prion connection. *Prion* **6**, 317-321

54. Mehrabian, M., Hildebrandt, H., and Schmitt-Ulms, G. (2016) NCAM1 Polysialylation: The Prion Protein's Elusive Reason for Being? *ASN Neuro* **8**

55. Mehrabian, M., Ehsani, S., and Schmitt-Ulms, G. (2014) An emerging role of the cellular prion protein as a modulator of a morphogenetic program underlying epithelial-to-mesenchymal transition. *Front Cell Dev Biol* **2**, 53

56. Yamashita, S., Miyagi, C., Fukada, T., Kagara, N., Che, Y. S., and Hirano, T. (2004) Zinc transporter LIVI controls epithelial-mesenchymal transition in zebrafish gastrula organizer. *Nature* **429**, 298-302

57. Brethour, D., Mehrabian, M., Williams, D., Wang, X., Ghodrati, F., Ehsani, S., Rubie, E. A., Woodgett, J. R., Sevalle, J., Xi, Z., Rogaeva, E., and Schmitt-Ulms, G. (2017) A ZIP6-ZIP10 heteromer controls NCAM1 phosphorylation and integration into focal adhesion complexes during epithelial-to-mesenchymal transition. *Sci Rep* **7**, 40313

58. Bedell, V. M., Westcot, S. E., and Ekker, S. C. (2011) Lessons from morpholino-based screening in zebrafish. *Brief Funct Genomics* **10**, 181-188

59. Stainier, D. Y. R., Raz, E., Lawson, N. D., Ekker, S. C., Burdine, R. D., Eisen, J. S., Ingham, P. W., Schulte-Merker, S., Yelon, D., Weinstein, B. M., Mullins, M. C., Wilson, S. W., Ramakrishnan, L., Amacher, S. L., Neuhauss, S. C. F., Meng, A., Mochizuki, N., Panula, P., and Moens, C. B. (2017) Guidelines for morpholino use in zebrafish. *PLoS Genet* **13**, e1007000

60. Wulf, M. A., Senatore, A., and Aguzzi, A. (2017) The biological function of the cellular prion protein: an update. *BMC Biol* **15**, 34

61. Daude, N., Wohlgemuth, S., Brown, R., Pitstick, R., Gapeshina, H., Yang, J., Carlson, G. A., and Westaway, D. (2012) Knockout of the prion protein (PrP)-like Sprn gene does not produce embryonic lethality in combination with PrP(C)-deficiency. *Proc. Natl. Acad. Sci. U. S. A.* **109**, 9035-9040

62. Young, R., Passet, B., Vilotte, M., Cribiu, E. P., Beringue, V., Le Provost, F., Laude, H., and Vilotte, J. L. (2009) The prion or the related Shadoo protein is required for early mouse embryogenesis. *FEBS Lett* **583**, 3296-3300

63. Daude, N., and Westaway, D. (2012) Shadoo/PrP (Sprn(0/0) /Prnp(0/0)) double knockout mice: more than zeroes. *Prion* **6**, 420-424

64. Mallucci, G., Dickinson, A., Linehan, J., Klohn, P. C., Brandner, S., and Collinge, J. (2003) Depleting neuronal PrP in prion infection prevents disease and reverses spongiosis. *Science* **302**, 871-874

65. Suzuki, T., Kurokawa, T., Hashimoto, H., and Sugiyama, M. (2002) cDNA sequence and tissue expression of Fugu rubripes prion protein-like: a candidate for the teleost orthologue of tetrapod PrPs. *Biochem Biophys Res Commun* **294**, 912-917

66. Aman, A., and Piotrowski, T. (2008) Wnt/beta-catenin and Fgf signaling control collective cell migration by restricting chemokine receptor expression. *Dev. Cell* **15**, 749-761

67. Komiya, Y., and Habas, R. (2008) Wnt signal transduction pathways. *Organogenesis* **4**, 68-75

68. Hernandez-Rapp, J., Martin-Lanneree, S., Hirsch, T. Z., Pradines, E., Alleaume-Butaux, A., Schneider, B., Baudry, A., Launay, J. M., and Mouillet-Richard, S. (2014) A PrP(C)-caveolin-Lyn complex negatively controls neuronal GSK3beta and serotonin 1B receptor. *Sci. Rep.* **4**, 4881

69. Matsuda, M., and Chitnis, A. B. (2010) Atoh1a expression must be restricted by Notch signaling for effective morphogenesis of the posterior lateral line primordium in zebrafish. *Development* **137**, 3477-3487

70. Solis, G. P., Schrock, Y., Hülsbusch, N., Wiechers, M., Plattner, H., and Stuermer, C. A. (2012) Reggies/flotillins regulate E-cadherin–mediated cell contact formation by affecting EGFR trafficking. *Mol. Biol. Cell* **23**, 1812-1825

71. Schmitz, M., Greis, C., Ottis, P., Silva, C. J., Schulz-Schaeffer, W. J., Wrede, A., Koppe, K., Onisko, B., Requena, J. R., Govindarajan, N., Korth, C., Fischer, A., and Zerr, I. (2014) Loss of Prion Protein Leads to Age-Dependent Behavioral Abnormalities and Changes in Cytoskeletal Protein Expression. *Mol. Neurobiol.*

72. Zhang, Y., Duc, A. C., Rao, S., Sun, X. L., Bilbee, A. N., Rhodes, M., Li, Q., Kappes, D. J., Rhodes, J., and Wiest, D. L. (2013) Control of hematopoietic stem cell emergence by antagonistic functions of ribosomal protein paralogs. *Dev. Cell* **24**, 411-425

73. Shum, E. Y., Jones, S. H., Shao, A., Dumdie, J., Krause, M. D., Chan, W. K., Lou, C. H., Espinoza, J. L., Song, H. W., Phan, M. H., Ramaiah, M., Huang, L., McCarrey, J. R., Peterson, K. J., De Rooij, D. G., Cook-Andersen, H., and Wilkinson, M. F. (2016) The Antagonistic Gene Paralogs Upf3a and Upf3b Govern Nonsense-Mediated RNA Decay. *Cell* **165**, 382-395

74. Salazar, S. V., and Strittmatter, S. M. (2017) Cellular prion protein as a receptor for amyloid-beta oligomers in Alzheimer's disease. *Biochem Biophys Res Commun* **483**, 1143-1147

75. Um, J. W., Kaufman, A. C., Kostylev, M., Heiss, J. K., Stagi, M., Takahashi, H., Kerrisk, M. E., Vortmeyer, A., Wisniewski, T., Koleske, A. J., Gunther, E. C., Nygaard, H. B., and Strittmatter, S. M. (2013) Metabotropic glutamate receptor 5 is a coreceptor for Alzheimer abeta oligomer bound to cellular prion protein. *Neuron* **79**, 887-902

76. Westerfield, M. (2000) *The Zebrafish Book. A Guide for the Laboratory Use of Zebrafish (Danio rerio)*. University of Oregon Press, Eugene, OR

77. Meeker, N. D., Hutchinson, S. A., Ho, L., and Trede, N. S. (2007) Method for isolation of PCR-ready genomic DNA from zebrafish tissues. *Biotechniques* **43**, 610, 612, 614

78. Bustin, S. A., Benes, V., Garson, J. A., Hellemans, J., Huggett, J., Kubista, M., Mueller, R., Nolan, T., Pfaffl, M. W., Shipley, G. L., Vandesompele, J., and Wittwer, C. T. (2009) The MIQE guidelines: minimum information for publication of quantitative real-time PCR experiments. *Clin Chem* **55**, 611-622

79. Baraban, S., Dinday, M., Castro, P., Chege, S., Guyenet, S., and Taylor, M. (2007) A large-scale mutagenesis screen to identify seizure-resistant zebrafish. *Epilepsia* **48**, 1151-1157

80. Baraban, S. C., Taylor, M. R., Castro, P. A., and Baier, H. (2005) Pentylenetetrazole induced changes in zebrafish behavior, neural activity and c-FoS expression. *Neuroscience* **131**, 759-768

81. Bhinder, G., and Tierney, K. B. (2012) Olfactory-Evoked Activity Assay for Larval Zebrafish. in *Neuromethods*, Humana Press, Totowa, NJ. pp 71-84

82. deCarvalho, T. N., Akitake, C. M., Thisse, C., Thisse, B., and Halpern, M. E. (2013) Aversive cues fail to activate fos expression in the asymmetric olfactory-habenula pathway of zebrafish. *Front Neural Circuits* **7**, 98

FOOTNOTES

This work was supported by operating grants to WTA from the Alberta Prion Research Institute – Alberta Innovates BioSolutions and the Alzheimer Society of Alberta & Northwest Territories. PLAL was supported by studentships from Alzheimer Society of Canada and Alberta Innovates Health Solutions.

The abbreviations used are: APP, Amyloid-β Precursor Protein; dpf, days post-fertilization; HRM, high resolution melt analysis ; mGluR5, metabotropic glutamate receptor 5; MO, morpholino; mRNA, messenger RNA; NCAM, neural cell adhesion molecule; PLL, posterior lateral line; *Prnp*, mouse prion gene; *prp1*, zebrafish prion gene paralog 1; *prp2*, zebrafish prion gene paralog 2; PrP^{C}, normal cellular prion protein; PrP^{Sc}, misfolded scrapie prion protein; PTZ, convulsant pentylenetetrazole; RT-qPCR,

Reverse Transcriptase Quantitative PCR; SEM, standard error of the mean; TALENs, Tal Effector Nucleases; WT, wild type; ZIP, Zrt- Irt-like Protein;

FIGURE LEGENDS

Figure 1. Two stable mutant lines of *prp1*$^{-/-}$ zebrafish were engineered and both lack overt developmental phenotypes. A. Targetted mutagenesis of the *prion protein 1* (*prp1*) gene via TALENs resulted in deletions within the first 50 bp of the translation start site. The coding region of the *prp1* gene (grey box) is within a single exon, homologous to the mammalian *PRNP* gene structure; approximately 4.25 kb of chromosome 10 is schematized. TALENs were designed to cut the zebrafish genome specifically in the start of the *prp1* coding region within exon 2. Two frame-shift alleles were isolated: zebrafish with the *prp1*^{ua5003} allele have an 8 base pair deletion (Δ8bp) and zebrafish with the *prp1*^{ua5004} have a 19 bp deletion (Δ19bp). The predicted protein products of these mutants are truncated because both of these frameshifts lead to a stop codon early in each allele, and remaining peptides have no similarity to prion proteins. **B.** Heterozygous *prp1*$^{+/ua5003}$ and zygotic *prp1*$^{ua5003/ua5003}$ larvae are similar in appearance to wild type larvae at 50 hours post-fertilization. **C.** The predicted wild type (WT) Prp1 protein shares most predicted domains with mammalian prion protein (PrP^C), though they differ in length. All recognizable PrP^C domains are lost in the mature predicted protein products of these mutant fish (bottom). These include signal peptides (S), repetitive region, a central hydrophobic domain (H), a GPI anchor. Glycine zipper (GxxxG), disulphide bridge (S—S) and N-linked glycosylation sites. Putative proteins from the ua5003 allele and ua5004 allele have a signal peptide, followed by nonsense sequence (36 amino acids and 2 amino acids, respectively) and early stop codons; the signal peptide is cleaved off of the mature PrP^C protein.

Figure 2. Maternal zygotic *prp1*$^{ua5003/ua5003}$ and *prp1*$^{ua5004/ua5004}$ zebrafish are predicted to be nulls and have no overt phenotypes except being slightly smaller than wild type as larvae. A. Maternal zygotic *prp1*$^{ua5003/ua5003}$ and *prp1*$^{ua5004/ua5004}$ zebrafish larvae have no overt phenotypes at 50 hpf. **B.** The mean lengths of maternal zygotic *prp1*$^{ua5003/ua5003}$ larvae and maternal zygotic *prp1*$^{ua5004/ua5004}$ larvae are reduced by 3% and 2.5%, respectively, compared to *prp1*$^{+/+}$ larvae at 50 hpf. * $p<0.05$ with the Kruskal Wallis test. n refers to the number of zebrafish. **C-D.** Maternal zygotic *prp1*$^{ua5003/ua5003}$ (C) and maternal zygotic *prp1*$^{ua5004/ua5004}$ zebrafish (D) survive to adulthood and have no overt phenotypes compared to wild type fish. ***prp1* transcript abundance is reduced in both mutant alleles. E.** *prp1* transcript abundance was reduced by approximately 10-fold in 3dpf *prp1*$^{ua5003/ua5003}$ larvae compared to 3dpf wild type larvae. Data is normalized to the wild type fish. **$p=0.0027$ with the unpaired t-test. n refers to the number of biological replicates (15-20 larvae/biological replicate. See also Supplemental Figure S2A & E). **F.** *prp2* transcript abundance was not altered in *prp1*$^{ua5003/ua5003}$ larvae. **G, H.** *prp1* and *prp2* are both substantially decreased in compound maternal zygotic *prp1*$^{ua5003/ua5003}$;*prp2*$^{ua5001/ua5001}$ mutants. ***$p<0.001$ with the unpaired t-test. This dramatically reduced gene product abundance is also apparent when quantified by RNA-Seq (Supplemental Figure S11) and is complemented by lack of evidence for cryptic splicing of mutant transcripts (Supplemental Figures S10 & S11), all of which should be considered within the context that the predicted mutant PrP1 and PrP2 proteins lack all recognizable PrP^C domains (Figure 1).

Figure 3. Putative redundancy between zebrafish prion gene paralogs does not account for lack of overt phenotypes. A. Maternal zygotic compound *prp1*$^{ua5003/ua5003}$;*prp2*$^{ua5001/ua5001}$ mutants (bottom) have no overt phenotypes compared to wild type fish (top) at 50 hpf. **B.** The *prp1*$^{ua5003/ua5003}$;*prp2*$^{ua5001/ua5001}$ mutants have a mean length that is increased by approximately 2% compared to wild type fish. * $p=0.0123$ with the unpaired t-test. Sample size (n=) refers to the number of fish. **C.** Maternal zygotic compound *prp1*$^{ua5003/ua5003}$;*prp2*$^{ua5001/ua5001}$ mutants (bottom) survive to adulthood and have no overt phenotypes compared to wild type fish (top).

Figure 4. Neurodevelopment, as revealed by neuromast number, is altered in zebrafish prion mutants, and the *prp1* and *prp2* paralogs have opposing phenotypes. A. Schematic of the development of the zebrafish PLL at 48 hours post fertilization (hpf), when Prim I (solid red line) has completed its migration towards the tail. It originated as a placode posterior to the otic vesicle (o.v.). During its migration it deposited 5 lateral proneuromasts (L1-L5) and a stream of interneuromast cells on each side of the body. At about 40 hpf, PrimI reached the tip of the tail to produce 2-3 terminal neuromasts (Ter.). and a second primordium (dashed blue line) formed near the otic vesicle. This primordium deposited the first two dorsal neuromasts (D1 and D2) and the first two secondary neuromasts (LII.1 and LII.2) (35). **B.** Neuromasts at 72hpf. **C-D.** A 2 dpf cldnb:gfp *prp1*$^{+/+}$ wildtype larvae (left) has 6 trunk neuromasts, while a 2 dpf maternal zygotic cldnb:gfp *prp1*$^{ua5004/ua5004}$ mutant (right) has 4 trunk neuromasts (quantified in Supplemental Figure S12). **E. Loss of *prp2* increased neuromasts, whereas loss of *prp1* decreased neuromasts.** Loss of *prp2* rescued the defects caused by loss of *prp1*. **p<0.05, ***p<0.01, ****p<0.0001 with the Kruskal-Wallis test. Alternatively, these symbols represent **p<0.01, ***p<0.001, ****p<0.0001, calculated with one-way ANOVA. ns=not_significant. † refers to one instance where non-parametric statistics disagree with parametric statistics, as Kruskal-Wallis reports p=0.065 on this small sample size, however a biologically and statistically significant reduction in this abundance is apparent with larger sample size (as per Supplemental Figure S12), and by ANOVA and in the ua5003 allele. Sample sizes (n=) refers to the number of fish. Raw data plotted in panel E is provided in Supplemental Table S4, and endogenous alkaline phosphatase labeling was used to visualize these neuromasts.

Figure 5: Product of the prion gene *prp1* protects from seizures akin to its paralog *prp2* but through separate pathways. Seizures in zebrafish larvae responding to the convulsant pentylenetetrazole (PTZ) quantified as increased locomotor activity. **A.** Loss of *prp1* increases response to convulsant. Top: zebrafish larvae (4 days post-fertilization) were monitored in 96-well plate over the course of hours (representative movement during 2 minutes of PTZ exposure reported as red traces). Graph: Typical activity traces of two individual larvae are shown, one of each genotype, before and during presence of PTZ. A typical *prp1*$^{-/-}$ larvae (blue trace) has approximately double the activity of a typical wild type (black trace) –in these particular individuals the ratio of PTZ-induced activity relative to basal activity was 13.29 and 32.61 for wild type and *prp1*$^{-/-}$, respectively. **B.** Disruption of either prion gene paralog increases seizure susceptibility, represented here as the mean of many activity tracings from larvae before and during exposure of 10 mM PTZ. Lines represent mean activity as % change in pixels within each minute, and shaded ribbons display ±SEM. **C.** Applying PTZ in a dose-response format reveals loss of *prp1* significantly increases seizure susceptibility. Loss of *prp2* is more impactful on seizure susceptibility compared to loss of *prp1*. Concerted loss of *prp1* and *prp2* does not exacerbate seizure susceptibility and instead significantly reduces it compared to loss if *prp2* alone. **D.** Loss of *prp2* reduced baseline activity of zebrafish larvae, whereas loss of *prp1* did to not measurably impact basal activity. Average baseline activity for each individual recorded over one hour (lines represent mean with error bars reporting ± SEM). Data in B and C assessed by 2-way ANOVA, in D by 1-way ANOVA. Sample sizes (n=) represent number of larvae tested. Symbol * indicates statistically significant compared to wild type. Symbol # indicates statistically significant compared to *prp1*$^{-/-}$;*prp2*$^{-/-}$. One * or $^{\#}$ indicates p<0.05; two, p<0.01; three, p<0.001; four, p<0.0001. Allele ua5003 of *prp1* used throughout; see Supplemental Figure S8 for other allele. The same behavioural traces were used to calculate velocity as an alternate metric of seizure intensity, which broadly shows the same relationships (Supplemental Figure S7).

Figure 1

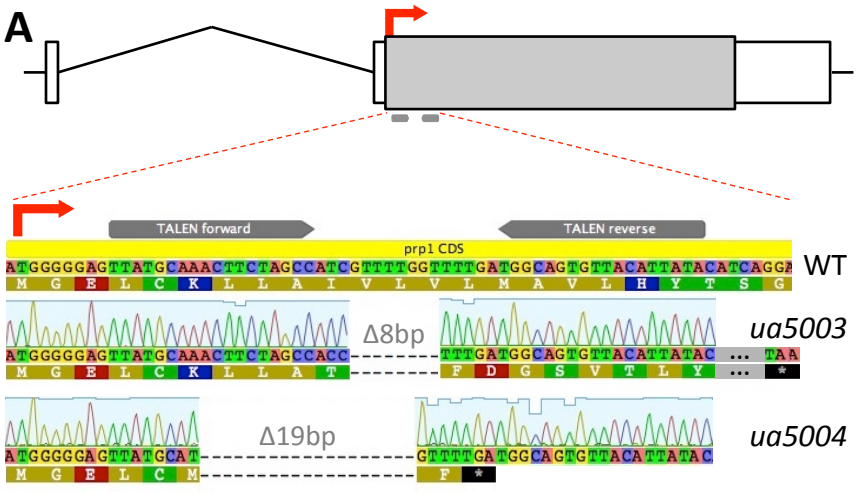
A
TALEN forward
TALEN reverse
prp1 CDS
WT
Δ8bp
ua5003
Δ19bp
ua5004

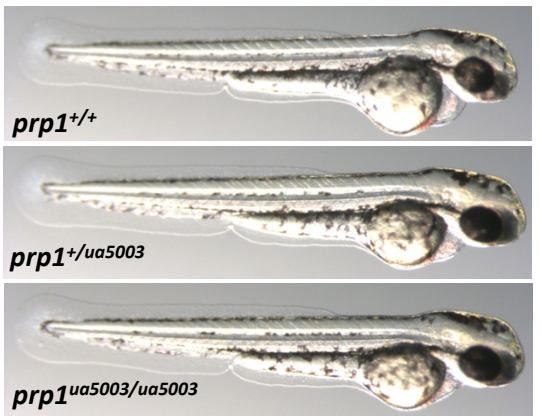
B
prp1+/+
prp1+/ua5003
prp1ua5003/ua5003

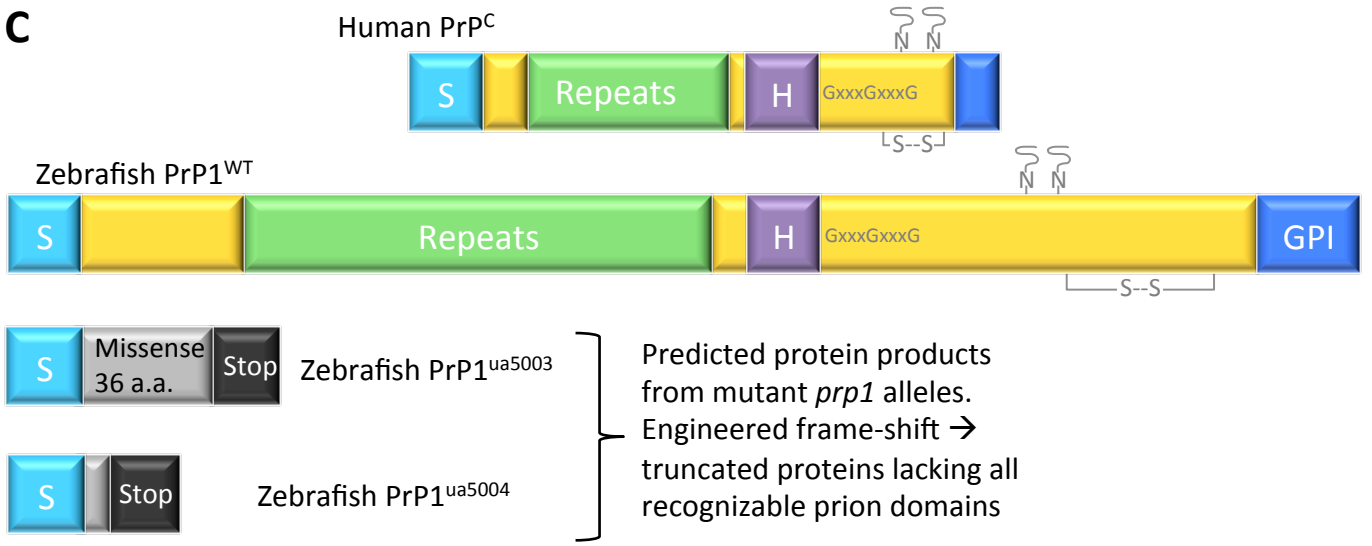
C
Human PrPC
S
Repeats
H
GxxxGxxxG
S--S
Zebrafish PrP1WT
GPI
Missense
36 a.a.
Stop
Zebrafish PrP1ua5003
Zebrafish PrP1ua5004
Predicted protein products from mutant prp1 alleles. Engineered frame-shift → truncated proteins lacking all recognizable prion domains

Figure 2

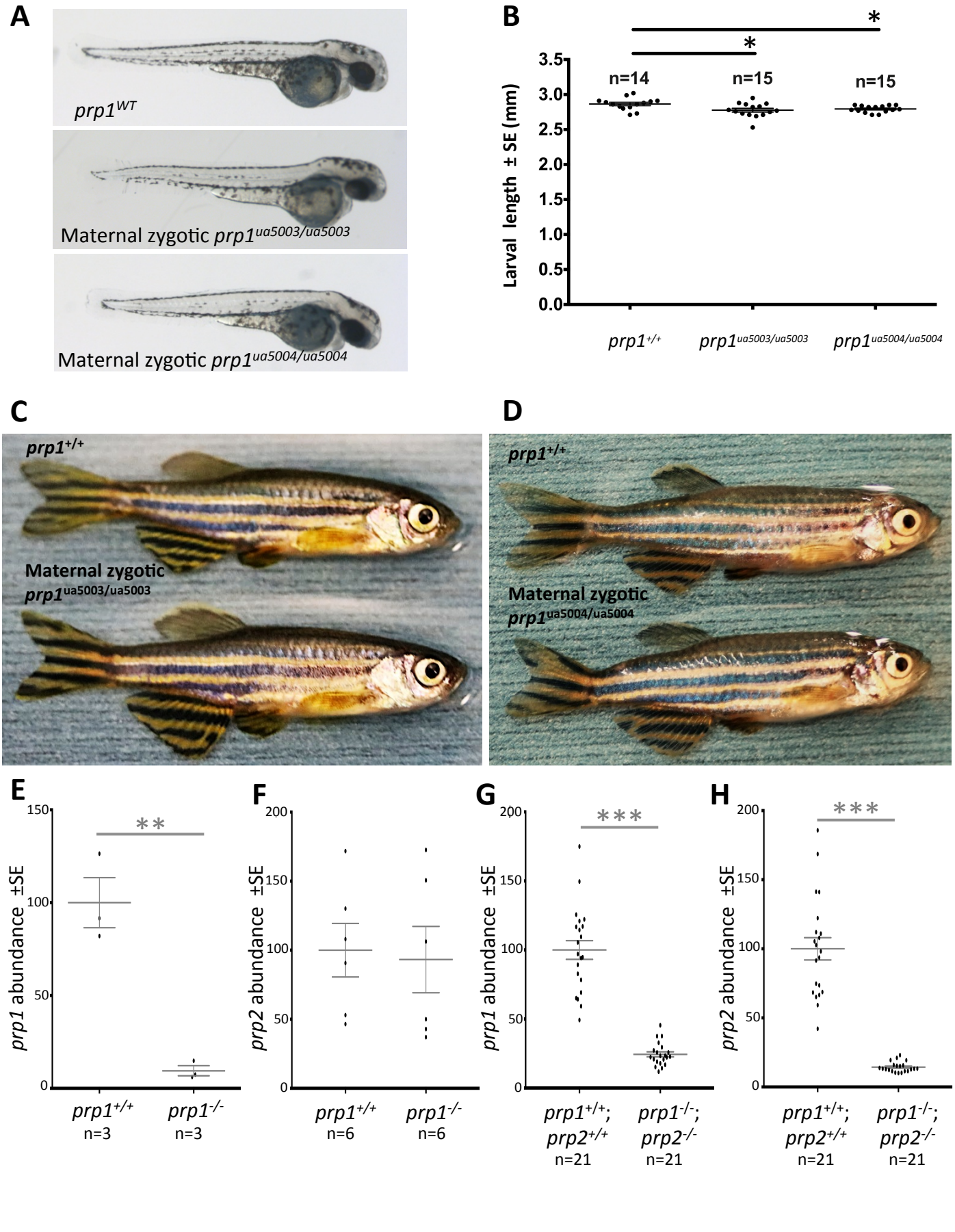
A
prp1WT
Maternal zygotic prp1ua5003/ua5003
Maternal zygotic prp1ua5004/ua5004
B
Larval length ± SE (mm)
3.5
3.0
2.5
2.0
1.5
1.0
0.5
0.0
n=14
n=15
n=15
*
*
prp1+/+
prp1ua5003/ua5003
prp1ua5004/ua5004
C
prp1+/+
Maternal zygotic
prp1ua5003/ua5003
D
prp1+/+
Maternal zygotic
prp1ua5004/ua5004
E
prp1 abundance ±SE
150
100
50
0
**
prp1+/+
n=3
prp1-/-
n=3
F
prp2 abundance ±SE
200
150
100
50
0
prp1+/+
n=6
prp1-/-
n=6
G
prp1 abundance ±SE
200
150
100
50
0
***
prp1+/+; prp2+/+
n=21
prp1-/-; prp2-/-
n=21
H
prp2 abundance ±SE
200
150
100
50
0
***
prp1+/+; prp2+/+
n=21
prp1-/-; prp2-/-
n=21

Figure 3

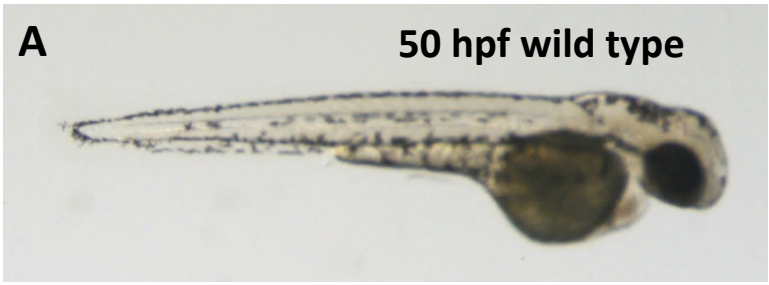
A
50 hpf wild type


50 hpf prp1ua5003/ua5003;prp2ua5001/ua5001

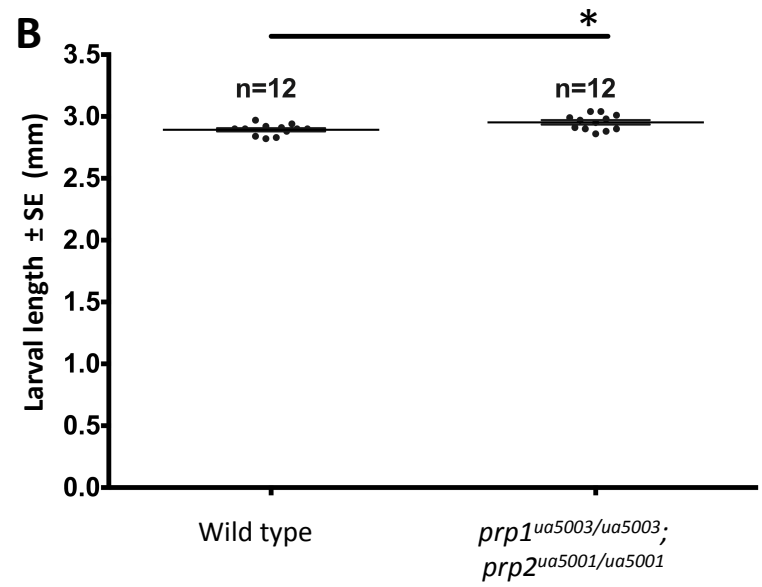
B
*
n=12
n=12
Larval length ± SE (mm)
3.5
3.0
2.5
2.0
1.5
1.0
0.5
0.0
Wild type
prp1ua5003/ua5003;
prp2ua5001/ua5001


C
Wild-type
prp1ua5003/ua5003;prp2ua5001/ua5001

Figure 4

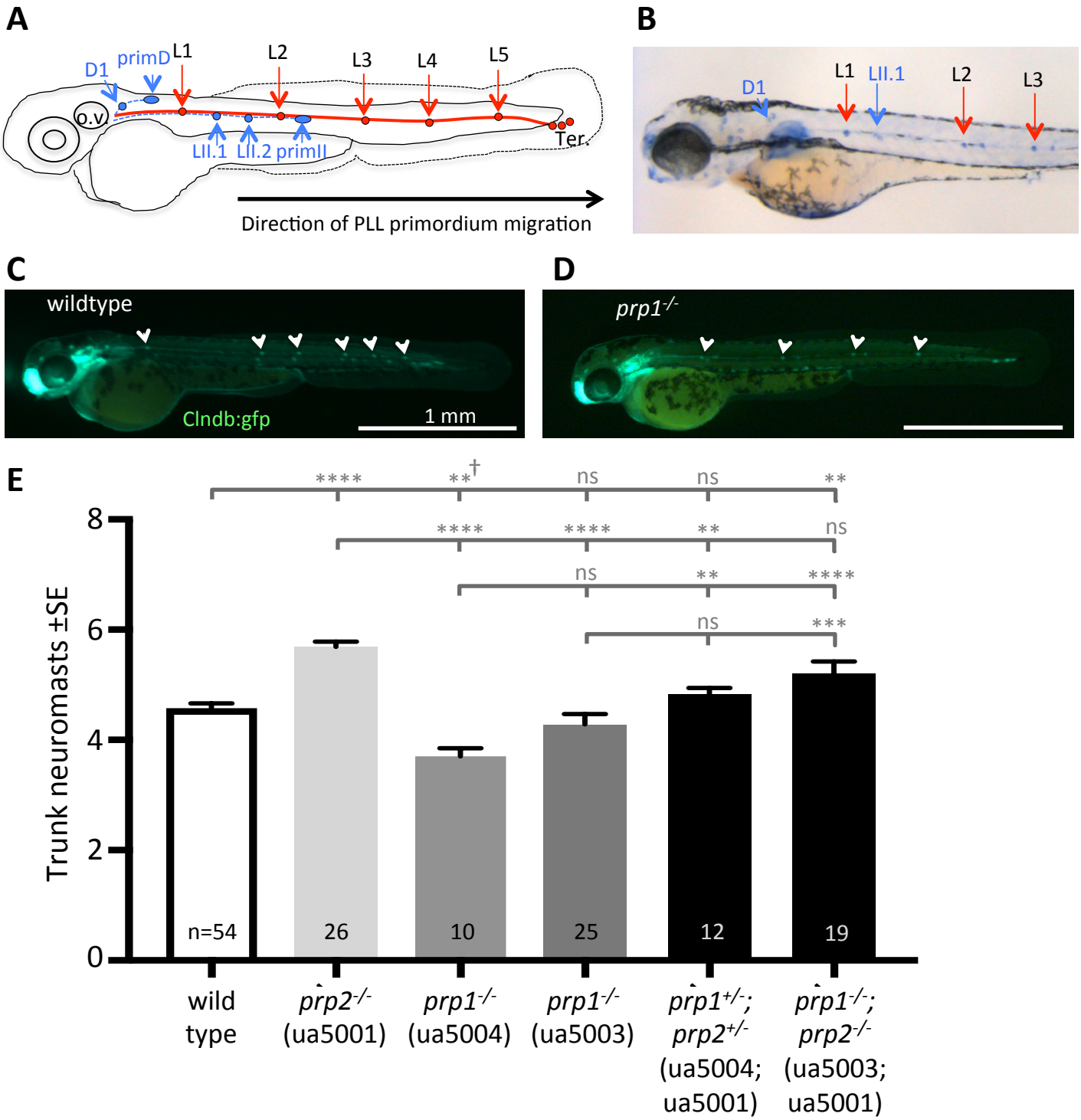
A
D1
primD
L1
L2
L3
L4
L5
o.v.
LII.1
LII.2 primII
Ter.
Direction of PLL primordium migration
B
D1
L1
LII.1
L2
L3
C
wildtype
Clndb:gfp
1 mm
D
prp1-/-
E
Trunk neuromasts ±SE
0
2
4
6
8
****
**†
ns
ns
**
****
****
**
ns
ns
**
****
ns
***
n=54
26
10
25
12
19
wild type
prp2-/- (ua5001)
prp1-/- (ua5004)
prp1-/- (ua5003)
prp1+/-; prp2+/- (ua5004; ua5001)
prp1-/-; prp2-/- (ua5003; ua5001)

Figure 5

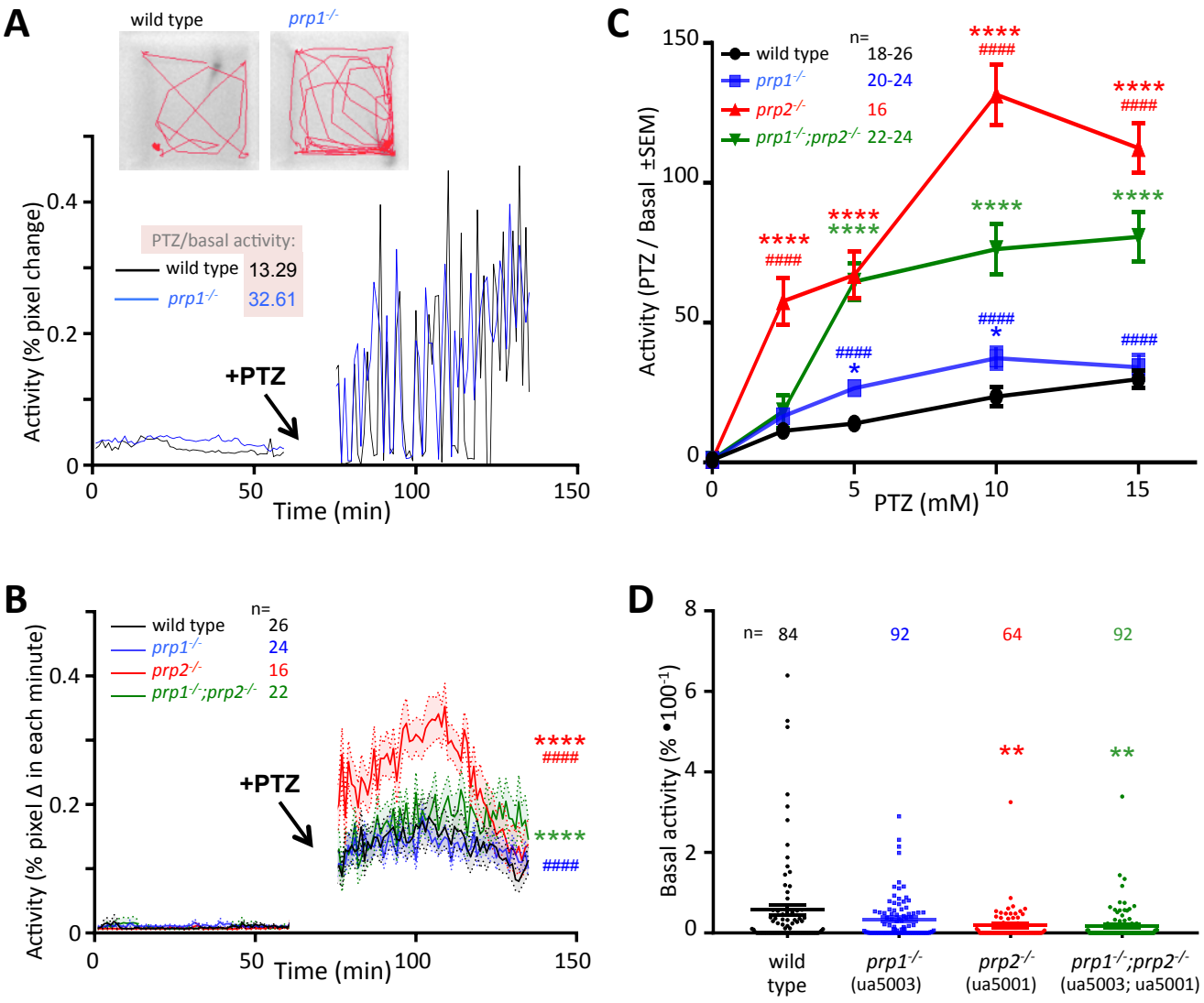
A
wild type
prp1-/-
PTZ/basal activity:
wild type 13.29
prp1-/- 32.61
+PTZ
Activity (% pixel change)
Time (min)
B
n=
wild type 26
prp1-/- 24
prp2-/- 16
prp1-/-;prp2-/- 22
+PTZ
Activity (% pixel Δ in each minute)
Time (min)
C
n=
wild type 18-26
prp1-/- 20-24
prp2-/- 16
prp1-/-;prp2-/- 22-24
Activity (PTZ / Basal ±SEM)
PTZ (mM)
D
n= 84 92 64 92
Basal activity (% •100-1)
wild type
prp1-/- (ua5003)
prp2-/- (ua5001)
prp1-/-;prp2-/- (ua5003; ua5001)

Prion gene paralogs are dispensable for early zebrafish development but have non-additive roles in seizure susceptibility

Patricia L.A. Leighton, Richard Kanyo, Gavin J. Neil, Niall M. Pollock and W. Ted Allison

J. Biol. Chem. published online June 14, 2018
